



UNIVERSIDAD NACIONAL AUTÓNOMA DE MÉXICO
DOCTORADO EN CIENCIAS (FÍSICA)
INSTITUTO DE CIENCIAS FÍSICAS

EFFICIENT QUANTUM TRANSPORT IN DISORDERED
INTERACTING MANY-BODY NETWORKS

TESIS
QUE PARA OPTAR POR EL GRADO DE:
DOCTOR EN CIENCIAS (FÍSICA)

PRESENTA:
HUGO ADRIAN ORTEGA ROSALES

TUTOR PRINCIPAL:
DR. LUIS BENET FERNÁNDEZ
INSTITUTO DE CIENCIAS FÍSICAS, UNAM

MIEMBROS DEL COMITÉ TUTOR:
DR. CARLOS FRANCISCO PINEDA ZORRILLA
INSTITUTO DE FÍSICA, UNAM

DR. THOMAS GORIN
UNIVERSIDAD DE GUADALAJARA

CIUDAD DE MÉXICO, OCTUBRE, 2017



Universidad Nacional
Autónoma de México



UNAM – Dirección General de Bibliotecas
Tesis Digitales
Restricciones de uso

DERECHOS RESERVADOS ©
PROHIBIDA SU REPRODUCCIÓN TOTAL O PARCIAL

Todo el material contenido en esta tesis esta protegido por la Ley Federal del Derecho de Autor (LFDA) de los Estados Unidos Mexicanos (México).

El uso de imágenes, fragmentos de videos, y demás material que sea objeto de protección de los derechos de autor, será exclusivamente para fines educativos e informativos y deberá citar la fuente donde la obtuvo mencionando el autor o autores. Cualquier uso distinto como el lucro, reproducción, edición o modificación, será perseguido y sancionado por el respectivo titular de los Derechos de Autor.

Contents

1	Introduction	1
1.1	On photosynthetic molecular complexes. The case of the Fenna-Matthews-Olson complex	1
1.2	On quantum buses. Efficient quantum graphs for the transfer of states	4
1.3	Thesis organization	6
2	Model and methods	7
2.1	Embedded random matrix ensembles for disordered interacting systems	7
2.1.1	From canonical RMT to the Embedded Gaussian Ensembles	8
2.1.2	Formal definition of Embedded Ensembles (EGE)	9
2.1.3	Centrosymmetry in the Embedded Gaussian Ensembles	11
2.1.4	Effect of centrosymmetry in the Embedded Ensemble	13
2.1.5	Eigenvalue densities for the Embedded Ensemble and the centrosymmetric Embedded Ensemble	16
2.1.6	Embedded Ensembles and their graph representation	18
2.2	Transport efficiency	19
2.3	Transport using Non-Equilibrium Green's functions method	20
2.3.1	Derivation of the Landauer formula	24
3	Closed systems: Best efficiency	27
4	Efficient open systems: Transport properties	32
4.1	Ensemble averaged transmission and current distributions	35

4.2	Statistics of the spectral decomposition of the transmission	40
4.3	Current as a function of the coupling to the contacts	43
5	Centrosymmetry breaking and robustness	45
5.1	EGE to csEGE transition	45
5.1.1	Analysis of the results	47
5.2	Centrosymmetry breaking	48
5.3	Centrosymmetry breaking in efficient csEGE networks	51
5.3.1	Parity breaking	51
5.3.2	Block perturbation in occupation number space	52
6	Conclusions and outlook	54
	Appendices	58
A	Bigger systems	59
A.1	Systems with $l = 8$ and $l = 10$ single-particle states	59
B	Publications	64

A mi madre.
Porque nunca hay que darse por vencidos.

Agradecimientos

Más allá de la dedicación y el tiempo invertido personalmente para terminar un posgrado, se trata de un esfuerzo social en donde entran en juego (al menos personalmente) la familia, mi novia, los amigos, la universidad en la que se estudia y todo el aparato educativo del país. Es por esto que en la clásica sección de agradecimientos quiero poner a aquellas personas que apoyaron mi formación académica.

Agradezco primeramente a mi madre, la cuál me ha enseñado a ser la persona que soy y que siempre ha estado como pilar fundamental en mi formación académica. A mi novia Maria de la Luz, muchas gracias por estar siempre conmigo, gracias por tu infinita paciencia y gracias por apoyarme siempre. Te amo profunda e infinitamente. Un agradecimiento póstumo a mi abuelo, el cuál me motivó desde pequeño esa curiosidad por la ciencia. A mi familia, en especial a Laura y a Miguel (de otro modo nunca hubiese pasado mis cursos de matemáticas en mi educación básica y no hubiese llegado tan lejos). A Héctor Ortega, gracias por apoyarme en los momentos difíciles que tuve que pasar lejos de toda mi familia.

En el ámbito académico quiero agradecer a mi tutor Luis Benet. Gracias por darme la formación como investigador y por la paciencia y ganas de enseñar Física. A Thomas Stegmann, por la valiosa enseñanza del trabajo sistemático (german style!). A Thomas Gorin y Carlos Pineda, por formar un comité tutorial de excelencia. A Thomas Seligman, por estar siempre al tanto de uno y apoyar académicamente a los estudiantes. A todos mis amigos del posgrado, que algunos se fueron y otros se quedaron, espero encontrarlos de nuevo. Las pláticas entre pares en las comidas y fiestas siempre son especiales, ya que he aprendido un tanto extra al compartir con gente joven y culta.

Al final pero no por menos importante (entre ellos a los que dan la lana y hacen posible que podamos enfocarnos a nuestras actividades académicas), a la UNAM y al técnico académico Reyes García por el servicio de cómputo. Finalmente agradezco apoyo del proyecto PAPIIT (IG-100616), al proyecto Fronteras de la Ciencia CONACyT 952, al proyecto CONACyT cb 219993, así como la beca CONACyT de doctorado.

Resumen

En esta tesis se estudian las propiedades de transporte en redes pequeñas de fermiones interactuantes. El sistema se modela usando los Ensembles Gaussianos Anidados (EGE). Con este modelo las interacciones entran como un parámetro k y con la cual hablamos de interacciones de k -cuerpos entre n -fermiones (sin espín) distribuidos en l -estados de una partícula. Analizamos dos tipos de ensembles: el EGE y este mismo ensemble con una simetría extra, conocida como centrosimetría (csEGE). En el contexto de transporte cuántico, la cuestión que se aborda es cuál de los dos ensembles (EGE vs csEGE) es más eficiente, ya sea en transferencia de estados, o en transporte coherente de fermiones en una red. Para comparar estos dos ensembles, estudiamos primero la eficiencia del transporte de estados en un sistema cerrado. Para ambos ensembles obtenemos las distribuciones de eficiencias. Podemos observar que la centrosimetría mejora significativamente la eficiencia del transporte cuando se compara con el EGE. También encontramos que, para obtener una buena eficiencia, el transporte debe ser considerado entre dos estados que están relacionados por la centrosimetría; para el EGE, no hay estados especiales que den una buena eficiencia: en principio todos los estados contribuyen a la distribución de eficiencia.

El siguiente paso es abrir el sistema y estudiar las propiedades de transporte del EGE comparado con el csEGE. El ancho de banda de la conductancia así como la corriente total promediada sobre el ensemble alcanzan sus valores máximos si el sistema está casi lleno $n \sim l - 1$ y la interacción es $k \sim n/2$. Para los casos $k = 1$ y $k = n$ el ancho de banda es mínimo. Mostramos que, una vez fijando l , para todos los posibles parámetros (del EGE o del csEGE) el transporte se mejora significativamente si se consideran los ensembles centrosimétricos (csEGE). En este caso la transmisión muestra numerosas resonancias de transporte perfecto. Analizando la transmisión usando la correspondiente descomposición espectral, encontramos que la centrosimetría induce fuertes correlaciones y mejora los extremos de las distribuciones. Esto suprime los efectos de interferencia destructiva en el sistema y causa resonancias en la transmisión libre de retro-dispersión (backscattering-free), lo cual mejora el transporte global. La distribución del total de la corriente para el csEGE tiene un pico muy grande que domina para $n = l - 1$, cerca de las corrientes más grandes observadas.

En la parte final, se estudia la transición del EGE al csEGE y el rompimiento de centrosimetría. En la transición EGE a csEGE consideramos, como función del

parámetro de transición ϵ , cómo la corriente promedio en el ensemble es mejorada. Se fijan los parámetros a $l = 6$ para el número de estados de una partícula y se consideran $n = 5$ partículas. El transporte de todos los ensembles mejora con interacción de $k = 3$ cuerpos, el mejor caso para obtener cantidades de transporte encontrado en toda la tesis. Para el EGE con $k = 1, 5$ y cualquier valor de k para el csEGE, la corriente promedio del ensemble es mucho mayor comparada con otros valores de k . Para $k = 2, 3, 4$, obtenemos resultados similares para la corriente promedio como función de ϵ . Cuando la perturbación (csEGE) tiene interacción $k = 1, 5$, encontramos que la corriente promedio puede decrecer. Mostramos que esto es una consecuencia de la modificación en las bandas de transmisión.

Estudiamos después el rompimiento de la centrosimetría, fijando $l = 6$ y $n = 5$. Como veremos, la centrosimetría se compone de dos partes: paridad y correlaciones. Para estudiar el rompimiento de la centrosimetría, analizamos de nuevo la corriente promedio sobre el ensemble como función del tipo de perturbación que rompe la centrosimetría. Para el rompimiento de paridad, y como función de k , la corriente promedio sobre el ensemble disminuye hasta alcanzar el valor cero. El caso que menos es afectado es $k = 3$, seguido de los casos $k = 2, 4$ y finalmente los peores casos son $k = 1, 5$. Como manera final de romper la centrosimetría, elegimos una perturbación general por bloques. Como en el caso previo, $k = 3$ es el caso menos afectado, seguido de $k = 2, 4$ y luego por $k = 1, 5$. Todos los ensembles alcanzan un valor mínimo en la corriente promedio, el cual es cuando la perturbación domina el transporte.

Nuestros resultados pueden ser usados en el contexto de redes pequeñas con pesos, donde los acoplamientos y las energías en sitio son aleatorias. Como veremos, las correlaciones juegan un papel fundamental ya que aumentan la eficiencia y las propiedades de transporte. Importantes aplicaciones de este tipo de redes se encuentran en sistemas cuánticos sobre diseño como los cables cuánticos, o en complejos fotosintéticos en bacterias o algas. Creemos que los resultados presentados en esta tesis pueden ser interesantes en los modelos de sistemas cuánticos, ya que generalizan el rango de las interacciones, los cuales pueden estar presentes cuando la energía es muy grande. En el contexto biológico, nuestros resultados pueden ser útiles en el estudio de transporte en complejos fotosintéticos, los cuales se sabe que operan de manera eficiente aún a temperatura ambiente, donde muchos grados de libertad están interactuando con el complejo molecular.

Abstract

In this thesis we study the transport properties in small interacting many-body fermionic networks. To model the system, we use the Embedded Gaussian Ensembles (EGE). With this model we can manipulate k -body interactions among n -spinless fermions distributed over l -single particle states. We analyse two types of ensembles: the EGE and this same ensemble with an extra symmetry, called centrosymmetry (csEGE). In the context of quantum transport, the question we address is which of the two ensembles (EGE vs csEGE) is more efficient, either in state transfer, or in coherent transport of fermions over a network. To compare these two ensembles, we study first the transport efficiency in a closed system. For both ensembles we obtain their respective efficiency distributions over the ensemble. We notice that centrosymmetry enhances significantly the transport efficiency when compared to the EGE. We also find that, in order to obtain a good efficiency, transport must be considered between two states related by centrosymmetry; for the EGE, there are no especial states that give a good efficiency: in principle, all states contribute to the efficiency distribution.

In the next step we open the system and study the transport properties in the EGE versus the csEGE. The conductance bandwidth as well as the ensemble-averaged total current attain their maximal values if the system is highly filled $n \sim l - 1$ and $k \sim n/2$. For the cases $k = 1$ and $k = n$ the bandwidth is minimal. We show that for all parameters the transport is enhanced significantly whenever the centrosymmetric ensembles (csEGE) are considered. In this case the transmission shows numerous resonances of perfect transport. Analysing the transmission by spectral decomposition, we find that centrosymmetry induces strong correlations and enhances the extrema of the distributions. This suppresses destructive interference effects in the system and causes backscattering-free transmission resonances, which enhance the overall transport. The distribution of the total current for the csEGE has a very large dominating peak for $n = l - 1$, close to the highest observed currents.

In the final part, we study the EGE to csEGE transition and centrosymmetry breaking. In the EGE to csEGE transition we consider, as a function of the transition parameter ϵ , how the mean current in the ensemble is enhanced. We fix $l = 6$ single-particle levels and $n = 5$ particles. All ensembles are enhanced with $k = 3$, the best case to obtain transport quantities throughout all this thesis. For the EGE cases with $k = 1$ and $k = 5$ and any value of k in the csEGE, the mean current

in the ensemble is largely enhanced compared to other values of k . For $k = 2, 3, 4$, we obtain similar results for the mean current as a function of ϵ . When the csEGE perturbation is $k = 1, 5$, we find that the mean current can decrease. We show that this is a consequence of the modification of the transmission bands.

Taking into account the results for finite systems ($l = 6$ and $n = 5$), we also explore centrosymmetry breaking, fixing $l = 6$ and $n = 5$. We believe this results will hold for other parameters like $l = 8, n = 7$ and $l = 10, n = 9$. As we shall see, centrosymmetry is composed of two parts: parity and correlations. To study centrosymmetry breaking, we analyse again the mean current over the ensemble as a function of the type of centrosymmetry-breaking perturbation. For the parity breaking, and as a function of k , the mean current over the ensemble diminishes until it attains zero value. The least affected case is $k = 3$, followed by $k = 2, 4$ and finally the worst cases are $k = 1, 5$. As a final way to break centrosymmetry we choose a general perturbation by blocks. As in the previous case, $k = 3$ is the least affected case, followed by $k = 2, 4$ and then by $k = 1, 5$. All ensembles attain a minimum value in the mean current, which is when the block perturbation dominates the transport. This minimum value is the characteristic transport over the perturbation by blocks.

Our results can be used in the context of small weighted networks, where the couplings and the on-site energies are random. We shall see that correlations increase the efficiency and the transport properties. Prominent applications of this type of networks are in engineered quantum systems like quantum buses, or in photosynthetic complexes of bacterias and algae. We believe that the results presented here can be interesting in the modelling of quantum buses, because they generalize the rank of interactions, which may be present when the excitation energy is high. In the biological context, our results can be useful in the study of transport across photosynthetic complexes, which are known that operate efficiently at room temperature, where many degrees of freedom are interacting with the molecular complex.

Chapter 1

Introduction

The advent of quantum technologies has opened new fields for studying quantum phenomena. If we focus specially in quantum transport problems, disorder is a property of the system that suppresses transport [1]. In recent years, the interest in transport problems present in complex systems [2] has demanded new theoretical descriptions that use disorder as a way to overcome quantum localisation. Two prominent examples are the study of excitonic transport in the Fenna-Matthews-Olson (FMO) molecular complex [3] (a molecular complex which is part of the photosynthetic process realized in green sulfur bacteria); and the engineered design of quantum buses, which are important components in a quantum computer [4]. One important ingredient in these systems is that they are highly efficient, meaning that an incoming state is propagated to a final state with high probability in a finite amount of time. The other important ingredient in these two motivational examples are the fact that both systems are finite. Throughout this thesis, we will be interested in studying efficient transport in finite disordered systems. Our global idea is to generalize these type of problems to study transport in inherently random interacting systems, which may represent systems at high energies for which an exact Hamiltonian description is no longer possible to study analytically (due to many-body interactions). In such cases, a statistical approach is proposed and it forms the core idea in which Random Matrix Theory is used in Physics [5–7].

1.1 On photosynthetic molecular complexes. The case of the Fenna-Matthews-Olson complex

As mentioned above, one of the characteristics of the photosynthetic complexes [8–29] is that all of them are finite systems. The relevant Hilbert spaces obtained from experimental results range from 6×6 [25, 26], to 14×14 [21, 24] dimensions. In particular, the FMO complex present in *Chlorobium tepidum* is composed by

three identical monomers (see Fig. 1.1) in which each one of them encloses seven *bacteriochlorophyll a* (BChla) molecules embedded in a protein cage of dimensions $45 \times 35 \times 15 \text{Å}^3$ [30] (this last element provides structural stability to the BChla molecules). The distance between two BChla molecules is typically of 11Å , and they interact via dipolar coupling [31]. Typical linear absorption spectra of the FMO shows an absorption range in the 200–900nm. The most prominent sub-band studied is the absorption band around 800nm [32]. Among these BChla molecules, there exist two especial sites called antenna and sink. The number and position of these particular sites varies from complex to complex (for example, it is considered that the FMO has one antenna and one sink in site 1 and 3, respectively). The function of the antenna is to capture an incoming photon, an excitation is formed and it travels between the BChla molecules until it reaches the sink. The sink is just an absorber where the excitation is converted later in useful energy. For the FMO complex, there is roughly only one excitation at a time that travels through the system. It is known by experiments that the maximal efficiency (in short, efficiency refers to how many photons are needed to generate one charge separation [30]) is very high in these type of systems. For the FMO complex, the experimental maximal efficiency is $\sim 95\%$ (see [30] and references therein).

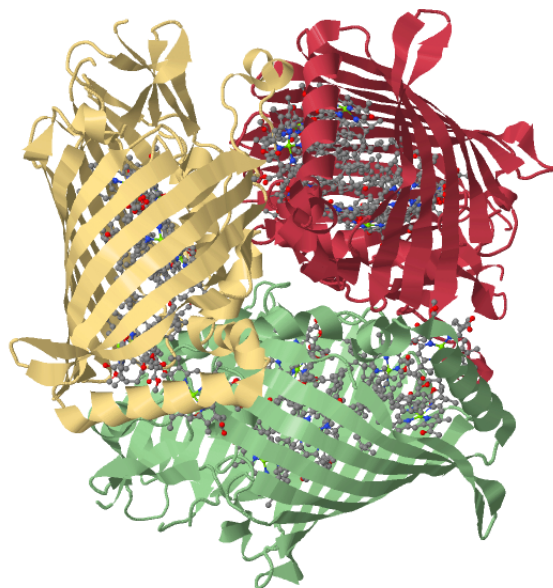


Figure 1.1: Crystal structure of the FMO protein from *Chlorobaculum Tepidum*, a model organism of green sulfur bacteria. The structure of the FMO consists of a trimer, formed by three identical monomers (protein cages in red, green and yellow) that each bind seven BChla molecules. One of this subunits is the main object of study in quantum transport communities and form one of the main motivations of this thesis (see main text for details). The figure was downloaded from <https://www.rcsb.org/pdb/home/home.do>

A quantum model for describing the FMO complex is to map the complex into a weighted disordered graph, in which each BChl_a molecule is the vertex of a graph. As we mentioned, there are dipole-dipole interactions and they constitute weighted edges between vertices. Finally, the specific position of the antenna(s) and sink(s) are chosen based on experimental observations. As these molecules operate at room temperature and they still present high efficiency rates, a sensible consideration in the theoretical models is to include some degree of noise (or disorder), which takes into account the overwhelming degrees of freedom that interact with the photosynthetic complex. As there is roughly one excitation at a time in the FMO complex, we can translate the graph model to a tight-binding Hamiltonian in which on-site energies and hopping rates are given by experiments. In order to obtain quantitative measures of transport across the FMO, the authors in [33, 34] proposed a quantum master equation (in Lindblad form) which describes an excitation travelling across the FMO from the antenna to the sink. The efficiency in this approach is the probability of trapping at the sink at a certain time. The noise is introduced as dephasing operators at each site which essentially randomizes the phase of the excitation at each site. The noise introduced in this way is a dynamical effect and it is precisely the mechanism to overcome the suppression of transport due to coherent evolution. As a function of the noise, the efficiency has essentially three behaviours. At low dephasing rate, the efficiency is around 80% with a transfer time of ~ 100 ps. At optimal dephasing rate, the efficiency becomes $\sim 100\%$ and a transfer time of ~ 5 ps. Finally, too much noise gives almost suppression of efficiency at times ~ 500 ps. This use of dynamical noise to overcome localisation and to improve transport is known as dephasing assisted transport. Further studies show that an equivalent classical system may attain similar efficiency [35]. These works described so far treat essentially a single excitation and they miss many-body effects.

Our approach in this thesis is different to the one described in the last paragraph. It is common knowledge that disorder suppresses transport (in the sense of Anderson localisation). We may ask ourselves what would be a necessary condition, under static disorder, to overcome localisation. In this direction, the notion of centrosymmetry is found to be useful to obtain good transport properties. Prominent examples are found in references [30, 36, 37]. These studies rely on random Hamiltonians, generated by ensembles of Random Matrices. With this type of models one can study interacting many-body systems (see for example [38–40]) and they form the main motivation in this thesis.

To summarize this section, molecular complexes involved in photosynthesis [41] (the FMO being the most studied of such complexes) display high efficiency, and this effect may be related to quantum behaviour. Therefore, transport can be analysed using quantum tools and quantum transport models [42]. It would be desirable to study transport in finite systems which are efficient even in the presence of disorder, or in other words, that despite of the disorder we can still obtain good transport properties.

1.2 On quantum buses. Efficient quantum graphs for the transfer of states

Quantum computers are devices that perform manipulations on data by making use of quantum phenomena, such as the superposition principle. From the algorithmic point of view, they hold the promise to overcome in reasonable finite time the solution of certain computational problems which in classical computation are “unsolvable” in finite time. For example, take the search of elements through a disordered database. For a database of length N , the Grover algorithm takes $O(\sqrt{N})$ steps to find the desired elements, see [43]. In contrast, a classical algorithm cannot be solved in fewer than $O(N)$ steps.

A quantum computer is composed by quantum processors. To transfer information between the processors, we need a device that can link processors. If the processors are composed by interacting spin chains, a reasonable proposal is that the buses are made up of the same quantum system. However the quantum bus cannot be composed by many particles, because we would be wasting computational power used in the transfer of information. The quantum bus is desired to have a finite and small number of particles. Suppose now that processor A encodes the result of a calculation in an input state $|A\rangle$, and that this state must be sent to a processor B. The state must be sent along the quantum bus before it reaches B; B then receives the output state $|B\rangle$. The idea is that $|\langle B|A\rangle|^2 \sim 1$, i.e. that the input state sent by processor A shall be received with high probability by processor B. Moreover, this state transfer must be achieved in a finite amount of time; the transfer of information between processors can be considered useless if they communicate at a very slow rate of time. The protocol described in this paragraph is the starting point of the seminal paper by Bose [44]. Bose’s results show, fixing the interactions among the spins, that the efficiency is $\geq 90\%$ for around ~ 20 spins. Incrementing the size of the chain shows an efficiency up to 70% for chains of 80 spins.

In this quantum bus model, particles can be considered as vertices in a graph and interactions as edges between nodes. Similarly to the molecular complexes, the problem is to transfer information from one input vertex to and output vertex. Which graph topologies are suitable for achieving that $|\langle in|out\rangle|^2 \sim 1$? Christandl et al [45, 46] showed that taking the k -fold Cartesian product (see [47] for its definition) of either a complete graph of dimension 2 (K_2) or a path graph of dimension 3 (P_3), it can be obtained Perfect State Transfer (PST) $|\langle in|out\rangle|^2 = 1$ in a finite amount of time. For example, the k -fold cartesian product of K_2 is a hypercube and if we calculate $|\langle in|out\rangle|^2$ in which $|in\rangle$ and $|out\rangle$ are antipodal vertices we find PST. If we use a path-collapsing argument [48], the hypercube is mapped to a weighted one dimensional chain again with PST. Before describing the construction of the mapping, recall that one way to describe a graph is via its adjacency matrix (see for example [49]). Since an adjacency matrix over a simple graph is symmetric, we can study

¹In a general graph, we are interested in the transfer probability from an input state $|in\rangle$ to an output $|out\rangle$. In the situation described in the previous paragraph, $|in\rangle = |A\rangle$ and $|out\rangle = |B\rangle$.

the dynamics over such graph by defining the Hamiltonian of the associated graph as its adjacency matrix H_A . Returning to the mapping, the idea is to construct a one-dimensional weighted graph from a simple graph which may be represented in \mathbb{R}^n and that we know beforehand that possess PST. For example, applying the 2-fold Cartesian product to K_2 we obtain C_4 , which may be seen as a square in \mathbb{R}^2 with all the sides equal to 1; if we apply the 3-fold Cartesian product to K_2 we obtain a graph which may be seen as the cube (in \mathbb{R}^3) with all sides equal to 1. The mapping that we will describe in the following works for any graph with the property that the vertices can be arranged in columns, without adjacency among vertices of the same column (as is the case in the hypercube). Further, we must require that each vertex at column j has the same degree, with the same incoming (from column $j - 1$ to j) and outgoing edges (from column j to $j + 1$). The next step is to construct the column basis, where each column state is defined as $|\text{col } j\rangle := \frac{1}{\sqrt{b_j}} \sum_{k=1, b_j} |v_{jk}\rangle$, where b_j are the number of vertices at column j , and $|v_{jk}\rangle$ labels vertex k at column j . In this column space, one calculates the representation of the Hamiltonian H_A . For the hypercube, the matrix elements for adjacent columns are $\langle \text{col } j | H_A | \text{col } j + 1 \rangle = \sqrt{j(N_C - 1)}$ and zero otherwise, where N_C is the number of columns. We have thus reduced the hypercube, which we know that possess PST, to a one-dimensional weighted graph (one-dimensional chain) with PST. This one-dimensional chain can be seen as a spin chain with nearest neighbour XY interactions, the interaction being $\sqrt{j(N - j)}$, where j is the label of the spin (counted from left to right) and N is the number of spins. It happens that this weighted one-dimensional graph fulfills centrosymmetry. This supports evidence that centrosymmetry is also present in ordered systems and, most importantly, that it is responsible of Perfect State Transfer. Perfect state transfer Hamiltonians can be achieved experimentally in spin chains with magnetic resonance techniques and in photonic lattices, see [51]. Another possibility to reach PST is by having n -bosons distributed in l single-particle levels and one-body interactions [50].

The PST chain described is a closed system. To be of any use, we must consider that every quantum system is interacting with its surroundings and the environment affects the behaviour of the central system. The inclusion of noise [52, 53], is a reasonable generalization of these type of systems. The question now is, which are the minimum requirements that one has to ask to the system in the presence of noise, in order to obtain almost PST? The answer of this question is our second motivation in this thesis.

1.3 Thesis organization

We have seen that finite quantum systems play important roles in either quantum transport, or in state transfer problems. Our aim in this thesis is to provide a model that in a way generalizes these type of problems. In order to do so, we will consider ensembles of random Hamiltonians with interactions. As we shall see, with the chosen Random Matrix model, we can consider transport problems from 1 to n particles distributed in l -single particle levels, with the extra degree of freedom that we can choose the interaction among the particles.

Chapter 2 is a self-contained section about the theoretical tools and methods used in the thesis. We begin by describing the random matrix model to simulate disordered networks with interactions, namely the Embedded Gaussian Ensembles for fermions (EGE). Next we establish how to define centrosymmetry in a model of fermionic interacting particles. Afterwards the definition of Transport Efficiency is put forward, as a theoretical measure of transfer rate between channels. To measure the transport in the steady-state through the network, we use the Non-Equilibrium Green's function method (NEGF). The central quantity that we analyse is the average current over the ensemble, which can be calculated using Landauer's formula. We provide a derivation of such formula. Chapter 3 analyses the Transport efficiency in the Embedded Ensembles, either with or without centrosymmetry. The transport properties in the steady-state are analysed in Chapter 4. Chapter 5 is concerned with centrosymmetry robustness. First we investigate the EGE to csEGE transition, in section 5.1.1. Then in section 5.3 we analyse two possible ways to break centrosymmetry. Finally in Chapter 6 we summarize the conclusions and outline future directions that remain unexplored in this thesis.

Chapter 2

Model and methods

In order to discuss a concrete disordered model, we will introduce in this section the necessary theory in which the model is built up and from which we draw the results (chapters 3, 4 and 5) and the Conclusions 6 of this thesis.

We begin by describing the Embedded Gaussian Ensemble (EGE) for fermions. We continue describing what is the centrosymmetry and how to apply it to the EGEs. Next we describe the quantity known in the literature as the efficiency [36] and with that we measure the time dependent performance of our system for a closed system (quantum system with unitary evolution). Then we describe the Non-Equilibrium Green's function method (NEGF) for which we investigate the behaviour of our system if we open it. In this case, the system will be considered efficient if it has high transmission probabilities.

2.1 Embedded random matrix ensembles for disordered interacting systems

We begin describing the Embedded Ensembles for fermions. There is also an analogous version for bosons, but we will concentrate on systems with spinless fermions. We will follow the review on Embedded Ensembles by Benet and Weidenmüller [54]. There is a relatively new reference [55] on Embedded Ensembles which contains also the general theory and some other applications.

Embedded Ensembles have their roots in what is known nowadays as canonical Random Matrix Theory (RMT for short), as introduced by Wigner in the 50's [56, 57]. Wigner's idea was to deal with the statistics of eigenvalues and eigenfunctions of many-body quantum systems. In short, if one wants to obtain the eigenergies of the nuclei, adequate nuclear models will provide the data in the low energy region.

However, it is known that the level density of such systems increase exponentially with the excitation energy. The problem becomes so complicated to solve analytically and numerically that a theoretical exact description of the problem becomes of no practical use. Rather, starting with Wigner, people tried to give a statistical description of the fluctuations of the energy levels. The basic idea was to build an ensemble of random matrices, which may describe at least statistically, eigenvalues of different nuclei. As we shall see, such RMT fall into three categories and take into account global symmetry properties of quantum systems. This statistical description was found to be appropriate because it describes individual nucleus like ^{166}Er [58] (obtained from experiments). In fact, if one builds an ensemble of energy levels from different nuclei available from experiments, one can confirm that the fluctuation measures coincide with one of the canonical ensembles in RMT (specifically with the Gaussian Orthogonal Ensemble, see the next section for its definition). The experimental ensemble is known as the Nuclear Data Ensemble and it is one of the first hallmarks of the importance of RMT in Physics. The importance of RMT goes well beyond nuclear physics, and it is precisely its character of universality that makes it so useful. Some examples where it has found application are in atoms and molecules, quantum chaos, disordered mesoscopic systems, QCD [6], wireless communications [59] and time series [60]. Even the distribution of primes and the Riemann conjecture have been linked to RMT [7, 61]. Our contribution in the thesis falls in the use of random matrices for studying quantum transport in finite systems. Inspired by the atomic nuclei, random matrices naturally describes quantum many-body systems. Our aim is to give a quantitative ensemble description of transport properties of interacting fermions. Instead of dealing with particular problems, like the FMO or the quantum buses described earlier, the aim is to study a broad ensemble of systems which can be suitable described by RMT. Before bringing forward definitions and details that concern us, we point out to the interested reader to some references (some of them classical references in the field) that complement this brief description of RMT and its use in Physics. Please refer to [5–7, 55, 58, 62] and a couple of relatively new publications [63, 64].

2.1.1 From canonical RMT to the Embedded Gaussian Ensembles

We shall consider ensembles of Hamiltonian matrices in which every member in the ensemble can be represented as a stochastic matrix (i.e. the matrix elements are random variables independent identically distributed). RMT considers ensembles of random matrices classified by their symmetries, and in canonical RMT there are three types [58]. It is customary to label such symmetries with the parameter β , where this number may attain the values of 1, 2, 4. If the system is time-reversal invariant and invariant under rotations, then $\beta = 1$; the elements of the Hamiltonian matrix can be chosen real symmetric and the ensemble is known as the Gaussian Orthogonal Ensemble (GOE). If the system is not time-reversal invariant, then $\beta = 2$ and the elements of the Hamiltonian (Hermitian) matrix are complex

numbers, and the ensemble is called the Gaussian Unitary Ensemble. Finally, if the system is time-reversal invariant, not invariant under rotations, and if it has half-odd-integer total angular momentum, then $\beta = 4$, and the matrices are quaternion real [7]. This ensemble is known as the Gaussian Symplectic Ensemble (GSE). Since we are interested in study (time-reversal) spinless interacting fermionic systems, the suitable symmetry to describe the ensemble is $\beta = 1$, or systems invariant under time-reversal symmetry. It may be of interest considering the influence of transport in the presence of magnetic fields, in which $\beta = 2$ is the right symmetry to consider, but we will restrict ourselves only in the former case. To construct an ensemble of such matrices ($\beta = 1$), we can choose normal distributed elements in every entry of the matrix, such that the matrix is symmetric. The diagonal elements have twice the variance of the off-diagonal elements. As we shall see, RMT is a limit attained by the EGE. In this limit, the Hamiltonian represents all possible interactions between n fermions, if the system has n fermions. Does the results change significantly if the Hamiltonian of the system considers effectively one- or two-body particle interaction? The first steps towards the understanding of random few-body interactions was carried out by French and Wong [65], and by Bohigas and Flores [66]. They analysed numerically what is known as the Two-Body Random Ensemble (TBRE). They found numerically that fluctuation measures in the spectrum (like the nearest neighbour spacing distribution or the Σ^2 statistic), are similar to those obtained using the GOE (at least at the center of the spectrum) [67]. The major trouble is that this model is not amenable for analytical investigations. Because of this, Mon and French [68] introduced the Embedded Gaussian Ensembles (EGE). If there are n -fermions in the system, with this model is possible to go beyond one- and two-body interactions. In fact, it allows to investigate the range $1 \leq k \leq n$, of k -body interactions. It also allows analytical investigations, see for example [55, 69]. The range of interaction k plays an important role in this thesis, as we will describe in chapters 3 to 5, which is a parameter that does not appear in the GOE. We will show that there is a clear advantage (in the sense that the transport properties of the system change) when manipulating the fermionic k -body interaction.

2.1.2 Formal definition of Embedded Ensembles (EGE)

We consider a set of l degenerate (fermionic) single-particle states $|j\rangle$, with $j = 1, 2, \dots, l$. The associated creation and annihilation operators are a_j^\dagger and a_j , with $j = 1, \dots, l$. They obey the usual anti-commutation relations which characterize fermions. We define the operators that create a normalized state with $k < l$ fermions from the vacuum state as $\psi_{k;\alpha}^\dagger = \psi_{j_1, \dots, j_k}^\dagger = \prod_{s=1}^k a_{j_s}^\dagger$, with the convention that the indices are ordered increasingly $j_1 < j_2 < \dots < j_k$. The index α in the many-body operators labels the specific occupation given by the j_s , and simplifies the notation. The corresponding annihilation operator $\psi_{k;\alpha}$ is constructed analogously.

The random k -body Hamiltonian reads

$$H_k = \sum_{\alpha, \gamma} v_{k; \alpha, \gamma} \psi_{k; \alpha}^\dagger \psi_{k; \gamma}, \quad (2.1)$$

which takes into account interactions between k particles and moves up to k particles from two different fermionic states of the occupation number basis. The coefficients $v_{k; \alpha, \gamma}$ are randomly distributed independent Gaussian variables with zero mean and unit variance

$$\overline{v_{k; \alpha, \gamma} v_{k; \alpha', \gamma'}} = \delta_{\alpha, \gamma'} \delta_{\alpha', \gamma} + \delta_{\alpha, \alpha'} \delta_{\gamma, \gamma'}. \quad (2.2)$$

The Hamiltonian H_k acts on a Hilbert space spanned by distributing $n \geq k$ particles on the $l > n$ single-particle states. A complete set of states is given by the set $\{\psi_{n; \alpha}^\dagger |0\rangle | \alpha \in P\}$, where P is the set of all possible configurations in which we can arrange n fermions in l levels, α being one specific configuration. The dimension of the Hilbert space is $N = \binom{l}{n}$. This defines the k -body embedded Gaussian orthogonal ensemble of random matrices for fermions [54, 55]. Notice that $H_{k=2}$ is reminiscent of similar hamiltonians used in condensed matter physics, for example the Hubbard model. The interaction $k = 2$ involves in the sum in Eq. (2.1) terms that do not move particles, i.e. the diagonal terms which are similar to on-site interactions of two particles, terms that move exactly 1 particle, and terms that move exactly 2 particles.

By construction, the case $k = n$ is identical to the canonical ensemble of random matrix theory [6], i.e. to the Gaussian orthogonal ensemble (GOE). For $k < n$, the matrix elements of H_k may be identical to zero and display correlations. Zeros appear whenever no k -body operator exist that links together the n -body states. Correlations arise because matrix elements of H_k not related by symmetry may be identical. One could argue that interactions between $k \sim n$ particles are averaged out and not relevant. However, in the case $k = n$ the Hamiltonian (2.1) is identical to the Gaussian orthogonal ensemble (GOE) [6], which has minimum information [70]. Moreover, transport in biomolecules takes place on a sub-picosecond time-scale [71], where correlations between many particles can be relevant. This justifies to address all rank of interactions.

As we consider finite systems of l states occupied by n particles, one may look for particle-hole symmetries in the system. The Hamiltonian H_k may describe n particles as well as $l - n$ holes; yet, in the embedded ensembles such symmetry is of no practical use, see [72]. Briefly, applying the particle-hole transformation to H_k , the result is a Hamiltonian that consists of the sum of ranks $0, 1, \dots, k$ in the hole representation, instead of a single term of rank k . Put it differently, if one considers $n = l - 1$, one may expect that $k = 1$ display the same behaviour as $k = n$. The structure of the matrices in the ensemble in both cases is almost equal, the only difference is that for $k = 1$, the diagonal elements have a broader variance than those of $k = n$. This apparently minimal difference makes that the eigenlevel

density (which will be much relevant when studying transport quantities) displays different behaviour. For $k = 1$ the eigenlevel density is a Gaussian while for $k = n$ we obtain a semicircle (both centered at zero). As for $k = n$ the H_k is by definition a GOE, we observe a *kind of* particle-hole symmetry in this cases, i.e. results for the parameters $(k = n, n)$ and $(l - n, k = l - n)$ are identical.

2.1.3 Centrosymmetry in the Embedded Gaussian Ensembles

Centrosymmetry is an important concept that enhances the efficiency [36, 37, 50, 73, 74] (see next subsection for definitions) and also enhances transport properties of the system [74]. A symmetric $N \times N$ matrix A is centrosymmetric if $[A, J] = 0$, where $J_{i,j} \equiv \delta_{i,N-j+1}$ is the *exchange matrix* [75] or, equivalently, an anti-diagonal unit matrix. One can therefore construct a centrosymmetric matrix by imposing that a real symmetric matrix A commutes with J . Centrosymmetry is also known as “mirror symmetry” in the literature (e.g. [51]). This term is easy to grasp with the following example. Consider the weighted path graph P_n with n vertices [76]. Physically, a weighted path graph can be constructed for example using the tight-binding model $\mathcal{H} = \sum_i t_{i,i+1} |i\rangle \langle i+1| + h.c.$, the $t_{i,i+1}$ are the weights of the edges that connect pairs of vertices. Let the weights connecting a pair of vertices be t_1, t_2, \dots, t_{n-1} . If we impose $[\mathcal{H}, J] = 0$, then our weights have to fulfill $t_i = t_{N-i+1}$. This is akin of considering only the half of P_n , and then placing a mirror in front of it. We see that the weights precisely fulfill $t_i = t_{N-i+1}$, where N is the total number of vertices (see Fig. 2.1).

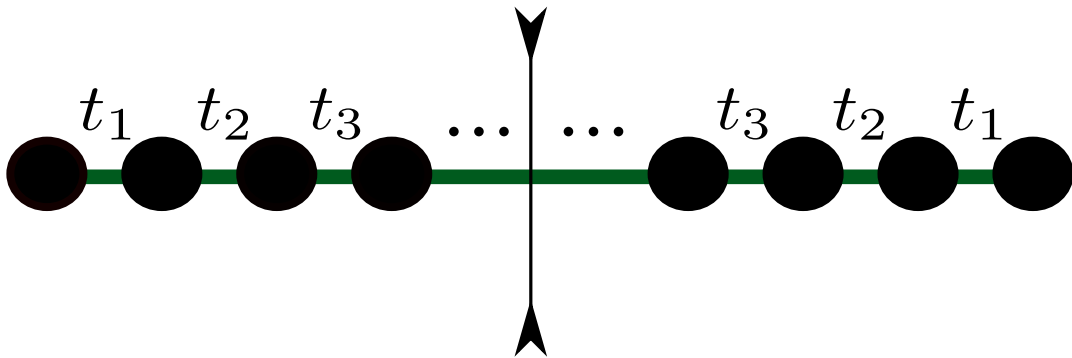


Figure 2.1: Weighted path graph P_n with centrosymmetry (mirror symmetry). The black-filled circles represent each vertex and the t_i the weighted edge between two vertices. The mirror symmetry is easily introduced in P_n if we cut half of the chain, place a mirror where we cutted (vertical black line), and then considering the other half of the chain being the one reflected by the mirror. The consequence is that the edges fulfill $t_i = t_{N-i+1}$, where N is the total number of vertices.

Imposing centrosymmetry to the k -body embedded ensembles is subtle. Considering the way in which we constructed H_k (Eq. (2.1)) and also following [50], it can be

introduced either at the one-particle level, which is the core for the definition of the k - and n -particle Hilbert spaces, at the k -body level, where the actual (random) parameters of the embedded ensembles are set, or at the n -body level, which defines the dynamics. The latter cases can be implemented following the procedure described in Ref. [75] (c.f. Lemmas 2(i) and 2(ii)), though it is not clear whether we should choose the k -body space or the n -body space. For example, the first lemma amounts to construct H (random!) with the block structure as

$$\begin{pmatrix} A & C^T \\ C & JAJ \end{pmatrix}, \quad (2.3)$$

where $A = A^T$ and C are block-random matrices of dimension $N/2 \times N/2$, T denotes the matrix transposition operation, the matrix C fulfills $C^T = JCJ$, and J is an exchange matrix of dimension $N/2 \times N/2$. Again, from only this lemma it is not stated if this construction is at the k - or n -particle level or at the one-particle level. Our definition of centrosymmetry takes into account the way in which we construct the EGE and as we shall see, it can be considered a generalization to centrosymmetry applied to fermionic operators. As we have stated that the one-particle states are the building blocks to construct both the k -body particle states and the n -body particle states, we shall define centrosymmetry at the one-particle level. Note that this approach yields a consistent treatment of more realistic situations, e.g. a system that includes a one-body (mean-field) term and a two-body (residual) interaction, $H = H_{k=1} + H_{k=2}$.

Considering that centrosymmetry is introduced at the one-particle level, we define it by $J_1 |j\rangle = |l - j + 1\rangle$ for $j = 1, 2, \dots, l$, whose matrix representation in the one-body basis is precisely the exchange matrix. For two fermions, we define $J_2 \psi_{2;j_1,j_2}^\dagger = J_1 a_{j_1}^\dagger J_1 a_{j_2}^\dagger = -\psi_{2;l-j_2+1,l-j_1+1}^\dagger$. The index 1 in J_1 emphasizes that the operator acts on the one-particle system, while the index 2 in J_2 emphasizes that J_1 acts on each one-particle operator. In the last equation we followed the convention that the indices are arranged in increasing order; then, the fermionic anticommutation relations impose a global minus sign, which can be safely ignored. This is generalized for k particles as

$$J_k \psi_{k;j_1,\dots,j_k}^\dagger = \prod_{s=1}^k J_1 a_{j_s}^\dagger = \psi_{k;l-j_k+1,\dots,l-j_1+1}^\dagger, \quad (2.4)$$

where we have dropped any global minus sign that may appear. We note that in general the matrix J_k , as defined by Eq. (2.4), may not be an exchange matrix. This follows from the possible existence of more than one state that is mapped by J_k onto itself; in this case, we shall say that J_k is a *partial* exchange matrix. As an example, considering $l = 4$ single-particle states and $k = 2$ -body interactions, the k -particle space has dimension 6. In this case, $J_2 \psi_{2;2,3}^\dagger = \psi_{2;2,3}^\dagger$ and $J_2 \psi_{2;1,4}^\dagger = \psi_{2;1,4}^\dagger$, ignoring the minus signs mentioned above, since under J_1 we have $|2\rangle \rightarrow |3\rangle$ and $|1\rangle \rightarrow |4\rangle$. Then, the entries in the J_2 matrix elements for these basis states are 1 in

the diagonal and J_2 is a partial exchange matrix. In contrast, for the case $l = 4$ and $k = 1, 3$ the resulting matrices J_1 and J_3 are exchange matrices. If the EGE posses centrosymmetry, either partial or full, we will call it centrosymmetric Embedded Gaussian Ensemble (csEGE).

2.1.4 Effect of centrosymmetry in the Embedded Ensemble

At this point it is instructive to see the effect of centrosymmetry for a concrete set of parameters. This same set of parameters will be chosen to analyse transport properties in the presence, or absence, of centrosymmetry. By choosing this set of parameters, the quantum systems that we analyse are comparable to some FMO and quantum buses. As we have described earlier (see section 2.1.3), depending on the parameters l -number of levels, n -number of particles, and k the rank of interaction, imposing the centrosymmetry at the one particle level we may generate partial or full centrosymmetry at the k -, or n - particle spaces.

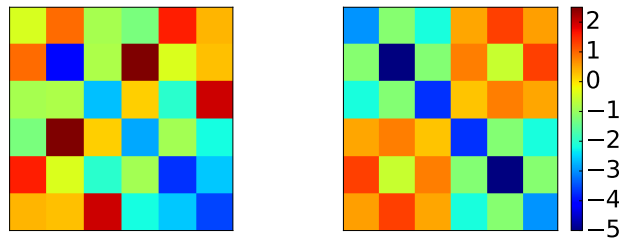


Figure 2.2: Comparison between a non-centrosymmetric matrix (left), and centrosymmetry (right). We show one realization with the parameters $l = 6$, $n = 5$ and $k = 2$. The color scale shows the weight of the matrix-elements as an aid to show the block structure when centrosymmetry is present (right), see Eq. (2.5).

In Fig. 2.2, we can observe the comparison between a member of the embedded ensembles with (right) and without (left) centrosymmetry. The parameters chosen are $l = 6$, $n = 5$ and $k = 2$. Each square in the matrices represents certain matrix entry $\langle \mu | V_k | \nu \rangle$. The Hilbert space has dimension $N_H = \binom{6}{5} = 6$ in both cases. In the non-centrosymmetric case (left), the matrix is only symmetric, while in the right case, the matrix is symmetric and commutes with the exchange matrix J . Notice that the centrosymmetric matrix has the block structure as given in the formula of Lemma 2 of reference [75], namely H can be written as

$$H = \begin{pmatrix} A & C^T \\ C & JAJ \end{pmatrix}, \quad (2.5)$$

which is the same as Eq. (2.3).

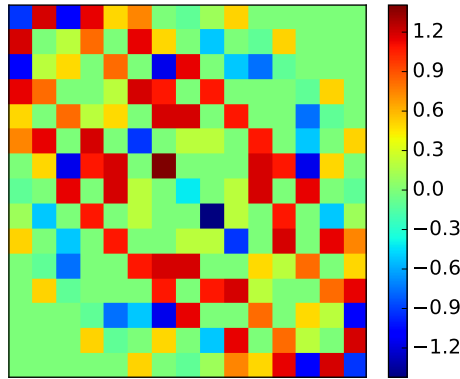


Figure 2.3: Partial centrosymmetry for a member of the ensemble with the parameters $l = 6$, $n = 2$ and $k = 1$. Notice that the non-centrosymmetric part is clearly showed at the center of the matrix. As in Fig. 2.2, the color code aids in showing the partial centrosymmetry of the matrix. At the center, the matrix is symmetric, while the outer structure fulfills centrosymmetry.

When centrosymmetry is only partial, our matrices in the ensemble are similar to the matrix depicted in Fig. 2.3. For this case the dimension is $N_H = \binom{6}{2} = 15$. As we saw in the example in section 2.1.3, there are more than one states that fulfill $J|\mu\rangle = |\mu\rangle$. These states are not centrosymmetric and they form a symmetric subset. As a result, the matrix representation of H will have centrosymmetric and non-centrosymmetric structure. The non-centrosymmetric structure is clearly seen in Fig. 2.3, at the center of the matrix.

As we have seen, the application of centrosymmetry to the one particle states does not imply that the resulting n -particle states, and therefore the EGE have full centrosymmetry. It depends on the number of states single-particle states, the number of particles and the rank of interaction. A full account for the presence partial (or full) centrosymmetry for $l = 6$ is shown in the Table 2.1.4

n	k	Type of centrosymmetry in k -space	Type of centrosymmetry in n -space
1	1	F	F
2	1	F	P
2	2	P	P
3	1	F	F
3	2	P	F
3	3	F	F
4	1	F	P
4	2	P	P
4	3	F	P
4	4	P	P
5	1	F	F
5	2	P	F
5	3	F	F
5	4	P	F
5	5	F	F

Table 2.1.3: Partial P (full F) centrosymmetry in the embedded ensembles for $l = 6$. The total number of particles is n and the rank of interaction is k . The type of symmetry depends on both n and k .

The first column labels the total number of particles n and the second the rank of interaction k . The third and four columns show the presence of partial or full centrosymmetry in the k - and n -particle spaces respectively. The k -particle subspace displays partial centrosymmetry for $k = 2, 4$ (and similarly for $n = 2, 4$); otherwise we have full centrosymmetry. We point out that partial centrosymmetry in k -space does not imply the same behaviour in the n -particle space.

As a final comment, we can consider the csEGE as less disordered system when compared to the EGE. In the k -particle space and in the presence of full centrosymmetry, the $v_{k;\alpha,\beta}$ matrix of Eq. (2.1) must commute with J (see Lemma 1 of Cantoni's paper [75]). The effect of imposing centrosymmetry is that the matrix has less than $\binom{l}{k}(\binom{l}{k} + 1)/2$ independent matrix elements (notice that $\binom{l}{k}(\binom{l}{k} + 1)/2$ is the typical number of independent identically distributed normal variables in the EGE [38]). This effect is also reflected in the transport efficiency, as well as the average current over the ensemble.

2.1.5 Eigenvalue densities for the Embedded Ensemble and the centrosymmetric Embedded Ensemble

As we have seen, the presence of partial or full centrosymmetry strongly depends on the choice of l , n and k . In this section we compare the eigenvalue statistics with the absence versus the presence of centrosymmetry (regardless if it is partial or full centrosymmetry).

In Fig. 2.4 we show the eigenvalue distribution for the Embedded Gaussian Ensemble (EGE, blue histograms) and the centrosymmetric Embedded Gaussian Ensemble (csEGE, bold-red histograms). The N_H indicates the dimension of the corresponding Hilbert space associated to a system with n -fermions distributed over l -single particle states. In blue and red numbers we indicate the associated variance $var(H)$ for the EGE and the csEGE, respectively. There are 10^4 realizations in each ensemble.

Notice that for a fixed n , the eigenvalue histograms suffer a transition from a Gaussian shape ($k = 1$) to a semicircle shape ($k = n$), which is to be expected for the EGE [72]. We observe that there are no significant changes when this case is compared to the csEGE. If we calculate the variance of the distribution $var(E)$, we can observe that for $n > 1$ and $k = 1$, the density is broader in the csEGE compared to the EGE. This trend is suppressed if we consider $k > 1$. In fact, both distributions behave approximately the same for any $n, k > 1$. We now discuss the variances $var(E)$. When $k \neq n$, we observe that the csEGE ensemble has a larger variance than the EGE case. When $k = n$, we obtain approximately the same dispersion for both types of ensembles. Finally, notice that when $k \approx n/2$, $var(E)$ attains its maximum value. This property will be important when we analyse time-independent transport properties. The dispersion when $k \approx n/2$ increases as a function of n , reaching its maximum value when $n = l - 1$ (for both ensembles).

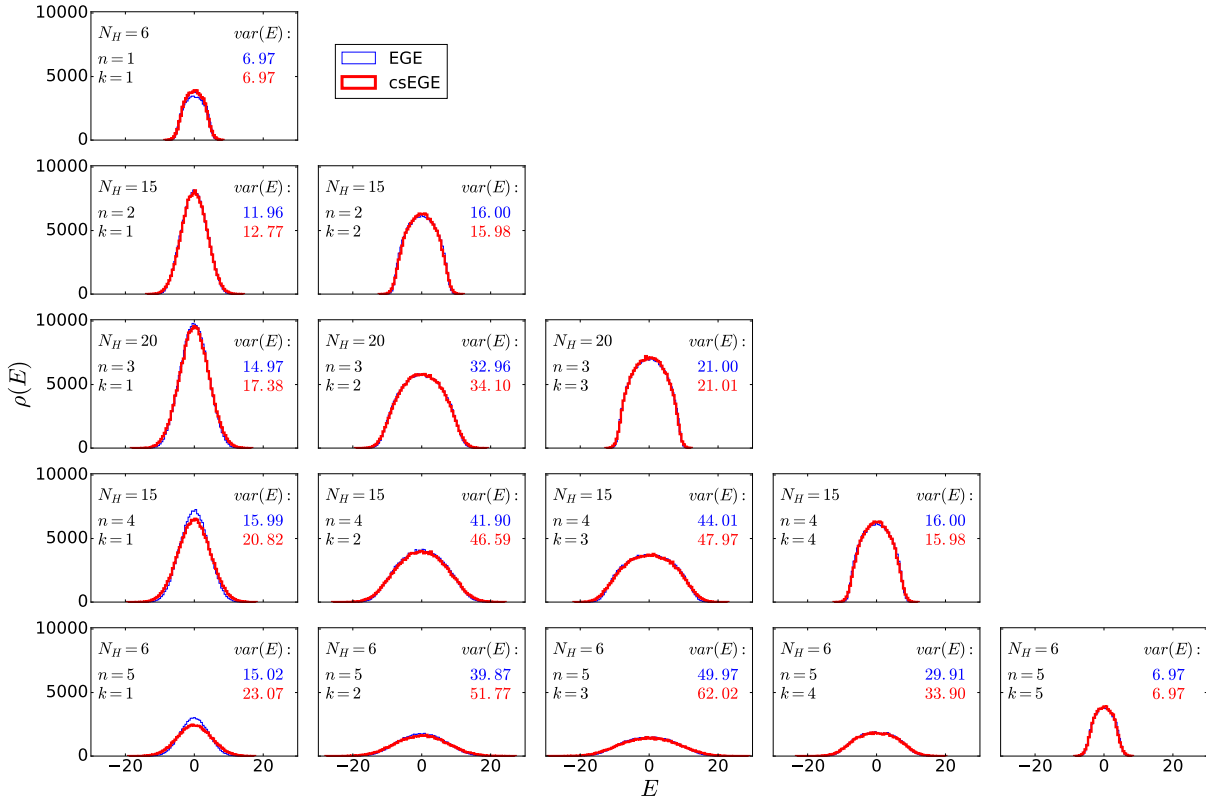


Figure 2.4: Eigenvalue density for the whole possible particles n and interactions k that can be distributed in $l = 6$ levels. Each column represents a fixed rank of interaction k and each row a fixed number of particles n , the specific values are shown in each subfigure. In blue we show the eigenvalue density for the EGE and in bold-red for the csEGE. N_H represents the Hilbert space dimension of distributing n -fermions in l -levels. We have indicated in blue and red numbers the variances $var(E)$ for the eigenvalues of the EGE and csEGE, respectively. There are 10^4 realizations in each ensemble. Notice that the biggest variance is when $n = 5$ and $k = 3$.

2.1.6 Embedded Ensembles and their graph representation

The EGE is amenable to be treated as a disordered network. In this section we will describe, given a certain number of single-particle states l , fermions n , and interaction k , how an disordered network can be built. This graphical representation is amenable to study when we introduce the transport efficiency Sec. 2.2 or transport quantities Sec. 2.3 (transmission probability or total current). As we shall see, in both approaches we have to choose two states, the input and output state. Among this two states we measure either Efficiency, or probability transmission, total current, etc.

Following [72], we can assign a graph representation to the EGE and to the csEGE. We assign to each many-particle state $|\mu\rangle$ a vertex μ , and to each non-diagonal matrix element $\langle\nu|H_k|\mu\rangle$ which is not identically to zero, a link connecting the vertices μ and ν . Each edge connecting two vertices has a weight given by the matrix element $\langle\nu|H_k|\mu\rangle$. The resulting graph for the EGE or the csEGE is a regular-weighted graph (see for example [49]). Figure 2.5 shows the weighted graph representation for a member of the EGE (left), and a member of the csEGE (right). Σ_{in} and Σ_{out} indicate two generic states from which we want to measure the performance of the graph. These two parameters will become clear in Chapter 3 and Chapter 4. Notice that both graphs are regular and have the same number of links. The difference between the two of them is that the graph with centrosymmetry has less independent random weights. This makes the graph on the right “more ordered”, compared to the EGE case. This feature is again manifested in the statistical transport properties as explained in subsequent chapters.

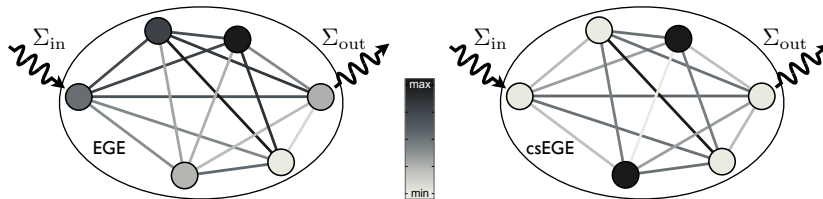


Figure 2.5: Weighted graph representation of the EGE (left) and csEGE (right) for a particular realization. Notice that both graphs are regular, but the one with centrosymmetry on the right, has less independent random parameters than the one on the left. Σ_{in} and Σ_{out} indicate two generic states from which we want to measure the performance of the graph.

In this thesis we are interested in the optimization of transport properties of a system that can be modelled by either EGE or csEGE. The graph approach allows us to fit our problem in the category of optimizations problems, such as *The network flow problem* (see for example [77], chapter 3 of the internet free edition). To the author’s knowledge, there are non algorithms treating the network flow problem when the edges are sampled from a random distribution, which we have in the graph representation of the EGE and csEGE. Centrosymmetry could be seen as an easy way to optimize the Network Flow Problem. As we shall see in sections 3 and

4, it is a desirable condition to have it in order to obtain good transport properties.

As a final comment, not all graphs are fully connected as in the Fig. 2.5. The connectedness of the graphs in the EGE and csEGE depends on l , n and k . When $n = l - 1$ (any k) the graphs are fully connected. In contrast, take for example $n = 3$. The total number of possible edges in a graph is $\binom{N}{2}$, where N is the number of nodes. The number of nodes is the same as the dimension of the single-particle basis. Therefore, when $l = 6$ and $n = 3$ then $N = \binom{6}{3} = 20$. The total number of edges in this case are $N * (N - 1)/2 = 190$. When $k = 1$, the number of missing edges is 100, for $k = 2$ is 10 and for $k = 3$ the number of missing edges is zero. The interested reader can find the formulas for calculating the connectivity of the graph of a EGE in the general case in [38]. Summarizing, the parameter k allows us to study transport properties from poorly connected graphs (generically when $k \ll n$), to fully connected graphs ($k \sim n$). As we shall see in the upcoming sections, the connectivity will play an important role in studying transport properties of these networks.

2.2 Transport efficiency

Efficiency is a quantity which measures maximum of the transfer probability between a pair of states at a certain time in a given time interval. It has been used in [36, 50, 78] to measure the performance of a disordered network, as the ones generated by Random Matrices. It has also been used in optimally designed networks, see for example [4, 44–46, 79]. The efficiency is the figure of merit for measuring transport probability in our closed system.

The transport efficiency from an input state $|\text{in}\rangle$ to an output state $|\text{out}\rangle$, is quantified as the maximum transition probability achieved among these states within a time interval $[0, T]$. The transport efficiency is defined as [36]

$$\mathcal{P}_{\text{in,out}} = \max_{t \in [0, T]} |\langle \text{out} | U(t) | \text{in} \rangle|^2. \quad (2.6)$$

The system is said to have perfect state transfer (PST) when $\mathcal{P}_{\text{in,out}} = 1$ [45]. In Eq. (2.6), $U(t)$ is the unitary quantum evolution associated with the Hamiltonian of the system and T is a reasonable time scale ($\hbar = 1$). At this point, we note that in Ref. [36] the time scale T was defined individually for each random matrix realization, essentially by the direct coupling matrix-element between the $|\text{in}\rangle$ and $|\text{out}\rangle$ states. For the embedded ensemble that we consider, such matrix element may be *identically* zero. We have thus opted for a fixed global time scale for all realizations of the ensemble. For each realization we have to construct the efficiency matrix, where each entry is precisely Eq. (2.6). As our Hamiltonian is real symmetric, the associated efficiency matrix is real symmetric (this matrix is known in the literature as the Gram matrix, see [80, 81]). For every efficiency matrix, we take its largest matrix-entry. This member, say $\mathcal{P}_{\gamma,\theta}$, is called the efficiency of its corresponding

realization. We shall analyse in Chapter 3 the averaged efficiencies and frequency histograms using $\mathcal{P}_{\gamma,\theta}$.

2.3 Transport using Non-Equilibrium Green's functions method

Non-Equilibrium Green's functions method (NEGF) is a formalism to study transport properties in nanostructures [82–85], molecular electronics [42] and mesoscopic systems [86, 87]. There is a wide variety of references about NEGF. Among the most popular, there are the books by Datta [86–88]. For a more mathematical oriented introduction, we refer the book by Economou [89]. For a detailed explanation using a scattering matrix approach, see the book by Mello and Kumar [90]. As expressed in many NEGF references (see for example [42]): “the central idea of the scattering approach, already put forward by Rolf Landauer in the late 50’s [91], is that if one can ignore inelastic interactions, a transport problem can always be viewed as a scattering problem”. In the following, we will discuss the model of an open system, and how to obtain the relevant transport equations used to analyse transport properties in both the EGE and csEGE. We will follow closely the reference [85].

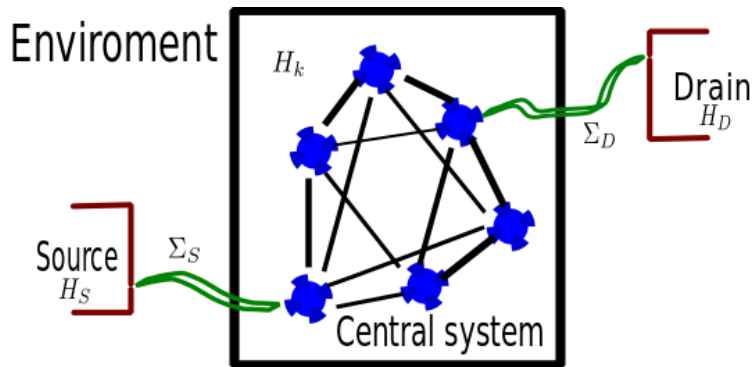


Figure 2.6: The transport problem analysed in this thesis. The central system is described by H_k , which in turn may be represented as a disordered-weighted graph. The enviroment is composed by the source and drain which are in equilibrium and characterised by their corresponding Fermi distributions. They are described by the Hamiltonians $H_{S/D}$, for the source and drain respectively. The system is coupled to the source and drain at certain nodes, described by the self-energies $\Sigma_{S/D}$.

From now on, we will refer as the central system the system described by l -single particle states, n -particles, and such particles interacting via the Hamiltonian H_k , Eq. (2.1). The enviroment is comprised by what is known as the contacts, which in turn are called source (their quantities described by a subscript S) and drain (denoted by D). In Fig. 2.6 we depict the case we already described. The purpose is to obtain effective transport equations on the central system, considering the “interaction” to the enviroment represented by the contacts.

Based on Fig. 2.6, we assume that the source and drain are in equilibrium and characterized by the Fermi distributions $f_{S/D} = f(E - \mu_{S/D})$, with chemical potentials $\mu_{S/D}$. There is a difference in the chemical potentials $\mu_{S/D}$, and therefore the system is driven out of equilibrium. This mechanism is responsible for the current flow.

The starting point for deriving the effective transport equations is as follows. We have already pointed out that the source and drain are in equilibrium. Without the presence of the central system (we will add it in a further step and there we will take into account the behaviour of the total system), the isolated contacts are described by their corresponding Hamiltonians $H_{S/D}$, and fulfill their own Schrödinger equations

$$(E - H_S) |\Psi_S\rangle = 0, \quad (2.7a)$$

$$(E - H_D) |\Psi_D\rangle = 0. \quad (2.7b)$$

We rewrite these equations as

$$(E - H_S + i\nu) |\Psi_S\rangle = |P_S\rangle, \quad (2.8a)$$

$$(E - H_D + i\nu) |\Psi_D\rangle = |P_D\rangle, \quad (2.8b)$$

where ν is an infinitesimal positive number, and $i\nu |\Psi_{S/D}\rangle = |P_{S/D}\rangle$. The terms $i\nu |\Psi_{S/D}\rangle$ and $|P_{S/D}\rangle$ represent the extraction and reinjections, of energy to the contacts, such that the contacts are always in equilibrium. In this last part, equilibrium means that the contacts are so large compared to the central system, that the presence of the latter does not alter the state in the contact. This means that, despite of the presence of the central system, the contacts are still characterised by $f_{S/D}$. Although the Schrödinger equation is mathematically unchanged from the set of Eqs. (2.7) to the set of Eqs. (2.8), the last set of equations allows a different point of view. In Eqs. (2.8), we consider that E is no longer an eigenvalue of the Hamiltonian, but an independent variable. This E gives the energy excitations $|P_{S/D}\rangle$ from external sources. In a similar manner, $|\Psi_{S/D}\rangle$ in Eqs. (2.7) is nonzero only for the eigenvalues, in Eqs. (2.8) the $|\Psi_{S/D}\rangle$ are non-zero for any energy and represent the response of the reservoirs to external excitations. When the central system is connected to the contacts, the energy levels in the contact are no longer delta peaks centered at its eigenvalues E_j , but rather there is a finite broadening which is the contribution of the contacts induced by $i\nu$. With these assumptions, the physical picture of transport through the central system is to investigate the transport of particles at any energy $E \in [\mu_D, \mu_S]$ from source to drain. Furthermore, the central system is viewed as an open system, due to the presence of $i\nu$.

We can study the dynamics of the full coupled system (central system + environment) by writing the corresponding Schrödinger equation. In matrix form it reads

$$\begin{pmatrix} E - H_S + i\nu & -\tau_S^\dagger & 0 \\ -\tau_S & E - H_k & -\tau_D \\ 0 & -\tau_D^\dagger & E - H_D + i\nu \end{pmatrix} \begin{pmatrix} \Psi_S + \xi_S \\ \phi \\ \Psi_D + \xi_D \end{pmatrix} = \begin{pmatrix} P_S \\ 0 \\ P_D \end{pmatrix}, \quad (2.9)$$

where the $\tau_{S/D}$ describe the interactions between the central system and the contacts. The states $|\Psi_{S/D}\rangle$ excite states $|\phi\rangle$ in the central system, which in turn excite states $|\xi_{S/D}\rangle$ in the contacts. The first and last row will lead to the expressions

$$|\xi_S\rangle = G_S \tau_S^\dagger |\phi\rangle, \quad (2.10a)$$

$$|\xi_D\rangle = G_D \tau_D^\dagger |\phi\rangle, \quad (2.10b)$$

where we have used Eqs. (2.8), and the fact that the states $|P_{S/D}\rangle$ are unaffected by the coupling. The $G_{S/D}$ are the Green's functions of the contacts, given by

$$G_{S/D} = (E - H_{S/D} + i\nu)^{-1}.$$

Using Eqs. (2.10) and the middle row of Eq. (2.9), we find

$$(E - H_k - \Sigma_S - \Sigma_D) |\phi\rangle = |P\rangle, \quad (2.11)$$

where the self-energies $\Sigma_{S/D}$ are given by

$$\Sigma_{S/D} = \tau_{S/D} G_{S/D} \tau_{S/D}^\dagger, \quad (2.12)$$

and the total excitation of the central system is

$$|P\rangle \equiv \tau_S |\Psi_S\rangle + \tau_D |\Psi_D\rangle. \quad (2.13)$$

Finally, for $|\phi\rangle$ we have

$$|\phi\rangle = G |P\rangle, \quad (2.14)$$

where G is the Green's function of the central system

$$G = (E - H - \Sigma_S - \Sigma_D)^{-1}. \quad (2.15)$$

We have thus reduced the Schrödinger equation of the total system to a single equation for the central system, which includes the coupling to the contact via the self-energies $\Sigma_{S/D}$. The self-energies are connected to the losses that the central system suffers by the contacts. They are typically non-Hermitian matrices, which shift the eigenvalues to the complex plane. The imaginary part of these eigenvalues are connected to the width of the resonances when we analyse the transmission function.

The self-energies $\Sigma_{S/D}$ are considered in the wide-band approximation, given by the equation

$$\Sigma_{S/D} = -i\eta\delta_{j,S/D}, \quad (2.16)$$

where η is a constant. This means that the energy scales related to the density of states of the leads are taken as constants for the whole conduction band of the central system. This way of modelling the contacts is used for example in [42, 85].

It remains to be shown how to obtain the total current through the central system system, known as Landauer formula. In order to do so, we will need a couple of extra definitions. The correlation function \mathcal{G} is defined as [42]

$$\mathcal{G}_{ij}(t, t') \equiv \langle a_i^\dagger(t') a_j(t) \rangle,$$

where a_i and a_i^\dagger are the usual fermionic annihilation and creation operators in i -th site. We now consider the substitution rule [85]

$$|i\rangle \langle j| \rightarrow \frac{1}{2\pi} \mathcal{G}_{ij}. \quad (2.17)$$

The spectral function is defined as

$$A(E) = 2\pi\delta(E - H) = -2\text{Im}(G), \quad (2.18)$$

where $\delta(x)$ is the Dirac delta function and G is the Green's function of the central system. The correlation functions of the contacts, which are assumed in equilibrium,

are related to the spectral function (for each contact) by [87]

$$\mathcal{G}_{S/D} = A_{S/D}(E)f(E - \mu_{S/D}), \quad (2.19)$$

where $f(E - \mu_{S/D})$ is the Fermi distribution that characterizes the corresponding contact. The functions $A_{S/D}$ are the spectral functions for the source and the drain, respectively. Now we calculate the density matrix of the central system

$$\begin{aligned} \rho &= |\phi\rangle\langle\phi| \\ &\stackrel{\text{Eq.2.14}}{=} G|P\rangle\langle P|G^\dagger \\ &\stackrel{\text{Eq.2.13}}{=} G\tau_S|\Psi_S\rangle\langle\Psi_S|\tau_S^\dagger G^\dagger + G\tau_D|\Psi_D\rangle\langle\Psi_D|\tau_D^\dagger G^\dagger \\ &\quad + G\tau_S|\Psi_S\rangle\langle\Psi_D|\tau_D^\dagger G^\dagger + G\tau_D|\Psi_D\rangle\langle\Psi_S|\tau_S^\dagger G^\dagger, \end{aligned} \quad (2.20)$$

where the last two terms are zero because there is no direct coupling between the reservoirs. By using the substitution rule for the contacts Eq. (2.19) we find

$$\begin{aligned} \mathcal{G} &= G\tau_S A_S \tau_S^\dagger G^\dagger f(E - \mu_S) + G\tau_D A_D \tau_D^\dagger G^\dagger f(E - \mu_D) \\ &= G\Gamma_S G^\dagger f(E - \mu_S) + G\Gamma_D G^\dagger f(E - \mu_D) \\ &= G\Sigma^{in} G^\dagger, \end{aligned} \quad (2.21)$$

where in the second equality we have defined $\Gamma_{S/D} = \tau_{S/D} A_{S/D} \tau_{S/D}^\dagger$, and in the last equality we defined the in-scattering function [87]

$$\Sigma^{in} \equiv \Gamma_S f_S + \Gamma_D f_D. \quad (2.22)$$

2.3.1 Derivation of the Landauer formula

We are now in position to derive the formula of the total current through the central system. We begin with the Liouville-von Neumann equation

$$\frac{d\rho}{dt} + \frac{i}{\hbar}[H, \rho] = 0, \quad (2.23)$$

where $\rho = |\phi\rangle\langle\phi|$, and $H = E - G^{-1} - \Sigma$ is the effective Hamiltonian for the central system ($\Sigma = \Sigma_S + \Sigma_D$). In the steady state, the first term of Eq. (2.23) vanishes.

If the system is not closed, then the commutator is proportional to the operator current through the central system

$$\hat{I} = \frac{ie}{\hbar}[H, \mathcal{G}], \quad (2.24)$$

where we have used the substitution rule Eq. (2.17) (from now on we set $e = 1$). By using Eq. (2.21) in this last expression and $H = E - G^{-1} - \Sigma$, we find

$$\begin{aligned} [H, G\Sigma_{in}G^\dagger] &= (E - G^{-1} - \Sigma)G\Sigma^{in}G^\dagger - G\Sigma^{in}G^\dagger(E - (G^{-1})^\dagger - \Sigma^\dagger) \\ &= G\Sigma^{in} + G\Sigma^{in}G^\dagger\Sigma - \Sigma^{in}G^\dagger - \Sigma G\Sigma^{in}G^\dagger \\ &= G\Sigma^{in} - \Sigma^{in}G^\dagger + G^m\Sigma^\dagger - \Sigma G^m. \end{aligned} \quad (2.25)$$

At this point we introduce the definition of the broadening matrix [87]

$$\Gamma \equiv i(\Sigma - \Sigma^\dagger), \quad (2.26)$$

and with Eq. (2.18); $A(E) = 2\pi\delta(E - H) = i(G - G^\dagger)$, taking the trace of Eq. (2.25), and using the cyclic property of the trace, we obtain

$$\begin{aligned} \text{Tr}[H, G\Sigma_{in}G^\dagger] &= \text{Tr}(G\Sigma^{in} - \Sigma^{in}G^\dagger + G^m\Sigma^\dagger - \Sigma G^m) \\ &= \text{Tr}(\Sigma^{in}A - \Gamma G^m). \end{aligned} \quad (2.27)$$

In this last step we have taken the trace of the current operator because we are looking for the total current through the central system, therefore the current takes the form

$$I(E) \equiv \text{Tr}(\Sigma^{in}A - \Gamma G^m), \quad (2.28)$$

where we have set $\hbar = 1$. This current must be zero, as it is stated by the continuity equation (2.23). The effective current through the central system could be obtained by analysing the total current through either the source, or the drain. The total current in the source is

$$I_S(E) = \text{Tr}(\Sigma_S^{in}A - \Gamma_S G^m). \quad (2.29)$$

As this is the current that is present through the central system, from now on we will simply call it the **total current**.

We rewrite the spectral function as

$$A = i(G - G^\dagger) = G(\Gamma_S + \Gamma_D)G^\dagger,$$

where we have used that: $i((G^{-1})^\dagger - G^{-1}) = \Gamma_S + \Gamma_D$. Using the second equality of Eq. (2.21) and this last expression for A , we can rewrite Eq. (2.29) to obtain

$$I_S = \int_{\mu_S}^{\mu_D} dE \text{Tr}(\Gamma_S G \Gamma_D G^\dagger), \quad (2.30)$$

where we have integrated over the accessible range of energies that are determined by the chemical potentials $\mu_{S/D}$ for source and drain respectively ($\mu_S < \mu_D$). This last equation is known as the **Landauer formula** [91]. Equation (2.30) is valid for temperature equal to zero, where the Fermi functions for the source and drain are determined by Heaviside functions, which are 1 up to the Fermi energy $E = \mu_{S/D}$, for source and drain respectively, and zero elsewhere. In section 4 we will use formula (2.30) in the infinite bias limit $(\mu_S - \mu_D) \rightarrow \infty$. The Landauer formula (2.30) could be rewritten as

$$I = \int T(E) dE,$$

where $T(E)$ is the transmission function

$$T(E) = \text{Tr}(\Gamma_S G \Gamma_D G^\dagger), \quad (2.31)$$

which is the probability of tunneling energy through the central system. The total current is taken as the analogous of the transport efficiency $\mathcal{P}_{\mu,\nu}$ (Eq. (2.6)), when the system is open and one wants to study transport in the steady-state.

Chapter 3

Closed systems: Best efficiency

In this chapter, we analyse the transport efficiency (or efficiency, for short) of networks generated by the embedded ensembles, with and without centrosymmetry. We recall that the transport efficiency is defined by Eq. (2.6)

$$\mathcal{P}_{\text{in,out}} = \max_{t \in [0, T]} |\langle \text{out} | U(t) | \text{in} \rangle|^2. \quad (2.6)$$

Inspired by the transport in photosynthetic complexes (which is known to take place in sub-picosecond timescales [71]), we ask the question on what is the transport efficiency in either the EGE or the csEGE at short time scales. In order to find which ensembles have the best efficiency, we analyse Eq. (2.6) by exhaustion, i.e. we fix the number of levels and then we sweep all the possible values that n and k may attain. For concreteness we analyse the case $l = 6$, varying the number of particles (fermions) from 1 to 5, and the rank of interaction from 1 to n . We consider the time interval (with $\hbar = 1$) $t \in [0, 15]$. As the quantity $\langle \mu | U(t) | \nu \rangle$ can have periodicities in the time interval chosen, we choose our efficiency as the first maximum at $t = t_1$ of the quantity $\langle \mu | U(t_1) | \nu \rangle$. We will focus in the best efficiencies in the ensemble. For each realization, we calculate its efficiency matrix with entries $\mathcal{P}_{\mu, \nu}$. Since H_k is symmetric, this matrix fulfills $\mathcal{P}_{\mu, \nu} = \mathcal{P}_{\nu, \mu}$. From the relevant $N \times (N - 1)/2$ efficiencies, we select the largest efficiency. We do this for every member of the ensemble. We consider 10^4 -realizations in each ensemble (EGE or csEGE). The results are shown in Fig. 3.1. In this plot the abscissa corresponds to the efficiency \mathcal{P} and the ordinate to the frequency of occurrence of certain efficiency $\mathcal{N}(\mathcal{P})$. The red (blue) histograms correspond to the csEGE (EGE). The red (blue) numbers correspond to the mean of the csEGE (EGE) plus/minus the standard deviation of the efficiency. Inspired by the FMO complex [3], the black straight line at 95% corresponds to the statistical benchmark, and is the same as the one reported in the literature [92], [30] and references therein. The criteria to decide if the ensemble in question is efficient is the following. If the efficiency distribution is in average around the benchmark of 95%, we will consider the ensemble as efficient.

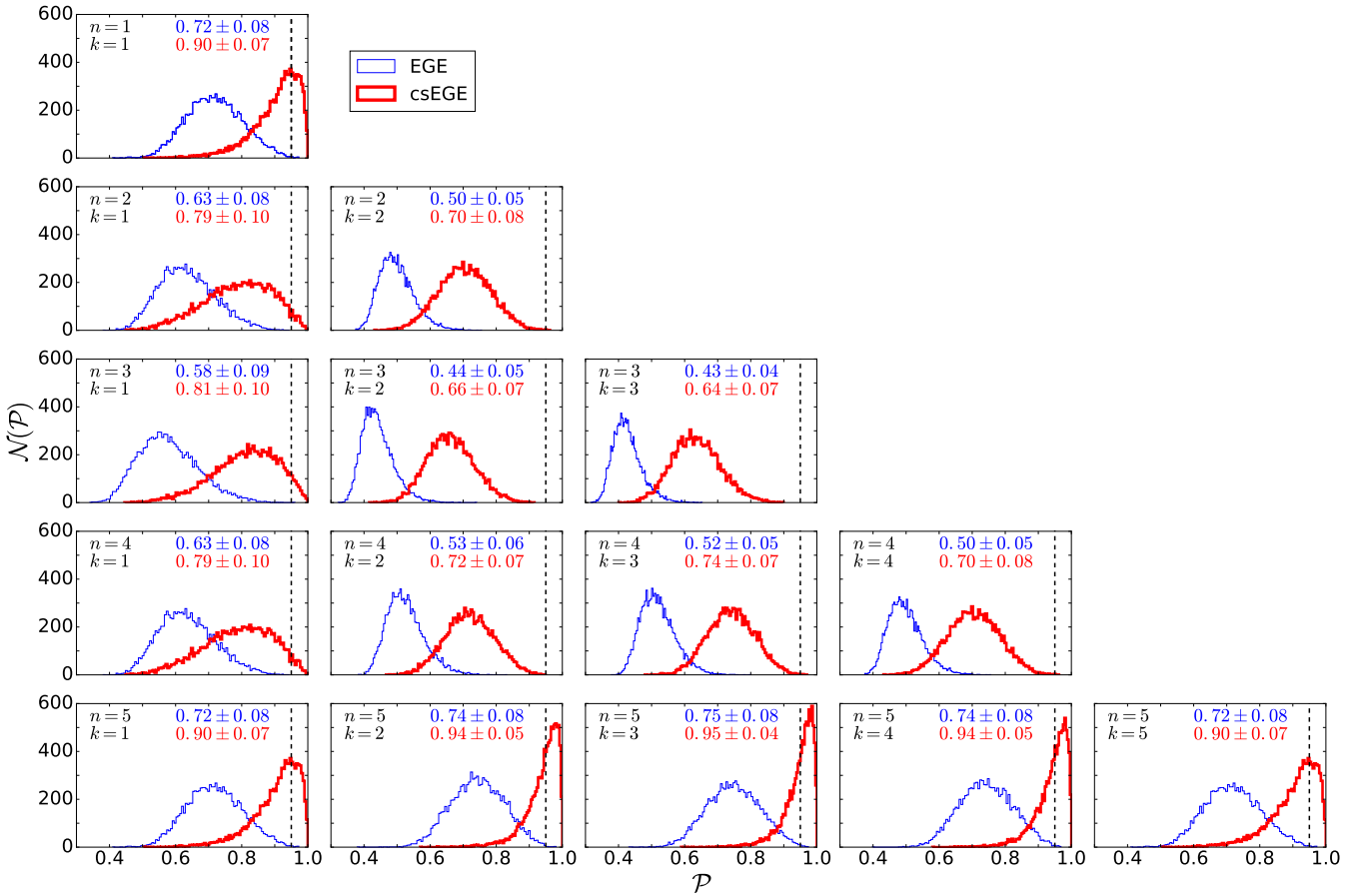


Figure 3.1: Efficiency distribution for the EGE and csEGE. The figure arrangement is the same as in Fig. 2.4. The x axis labels the efficiency \mathcal{P} and the y -axis the frequency that an efficiency has been obtained. The red histogram corresponds to csEGE and the blue histogram to EGE. In red (blue) numbers we plot the mean (\pm the standard deviation) efficiency over the ensemble. The dashed black line is the statistical benchmark, set at 95%. Notice that csEGE improves the efficiency rates in general, when compared to the EGE. The best cases are obtained when $n = l - 1 = 5$ and $k \sim n/2$.

The distributions in Fig. 3.1 reveal that for any (n, k) the csEGE is always closer to efficiency 1 than the EGE. Furthermore, the mean value of the distributions for the EGE (blue) and the csEGE (red) supports the fact that the csEGE is more efficient than the EGE. For all cases of averaged quantities of the EGE ensemble, we cannot reach the benchmark of 95%. The EGE distributions are spread at most 8% around their mean value (the spreading quantified by the standard deviation). If we fix n , both distributions (EGE and csEGE) display a transition as a function of k . For $n = 1, 2, 3, 4$ we find that the best efficiency corresponds to $k = 1$. As we tune the interaction k , the distributions tend to shift to the left (see how the mean efficiency changes as a function of k). For these values of n , looking at any row, the lowest efficiencies are found when $k = n$. Recall that by definition (see section 2.1.2), when $k = n$ the ensemble corresponds to either the GOE or the csGOE. This means that when $k = n$, for every member of the ensemble, its corresponding matrix elements are uncorrelated random variables. Compared to the cases with $k < n$, which have better efficiency, $k = n$ has too many independent parameters. This means that if we want better transport efficiencies, there must be correlations in the matrix elements of either EGE or csEGE (which in turn means that the k must be $k < n$). For $n = 1, 2, 3, 4$ and $k = 1$, the spreading of these distributions is bigger, when compared to other values of k . The case $k = 1$ for $n = 2, 3, 4$ essentially means two types of correlations in the matrix elements of every ensemble EGE or csEGE. We will focus in the case $n = 2$, but the same arguments apply to $n = 3, 4$ and the csEGE with $n = 2, 3, 4$. The first type of correlation is that many matrix elements will be identically zero, for $n = 2$ we have 45 such elements. The second relies on the allowed independent random variables that one may have in the ensemble. When $n = 2$, the dimension of the Hilbert space is $N_{n=2} = 15$. This means that we can have at most $15 \times 16/2 = 120$ independent random variables (because the matrices are real symmetric). From these we know that there are only $120 - 45 = 75$ -elements different from zero. As the $k = 1$ -body space has dimension $N_k = \binom{l}{k} = \binom{6}{1} = 6$, we can have at most 21 independent random elements. These 21-independent random variables from the k -particle space determine the 75-matrix elements in the n -body space. Therefore, these 75-matrix elements are not independent from each other and they are correlated via the independent elements in the $k = 1$ -particle space. The message is that these correlations are important in obtaining better transport efficiency. Any efficiency distribution with $n = 1, 2, 3, 4$, and $k \neq n$, is better than the case when $k = n$.

We will now discuss the case $n = 5$. Compared to other values of $n \neq 5$, the distributions and the average efficiency is better for $n = 5$. For $n = 5$ the distributions suffer a transition as a function of k (as in the case of other values of n), but while in the previous case, incrementing k was detrimental, here is beneficial up to $k = 3$. For $k = 4$ we find essentially the same values as for $k = 2$ and $k = 1$ is essentially the same as $k = 5$. The best efficiency distribution in all the parameter configuration is for $k = 3$, although the csEGE is better than the EGE. The csEGE has mean efficiency of 95%, and standard deviation of 4%. For the csEGE only, the efficiency distributions are optimal for $k = 2, 3, 4$, because all of them are around the 95% benchmark, and the standard deviation is at most of 5% in each one of them.

The reader may notice the symmetries in this figure for different values of n and k . The first symmetry that we explain concerns the definition of the EGOE (or csEGO) when $k = n$, and the dimension of the Hilbert spaces for different values of n . Remember that by definition, when $k = n$, the ensembles are either GOE or csGOE. Recall also that the Hilbert space dimension for n -particles is $N_n = \binom{6}{n}$. By virtue of the binomial coefficient, $N_1 = N_5$ and $N_2 = N_4$. Therefore we have essentially two dimensionally equivalent GOE (csGOE) ensembles for $n = 1, 5$ - and $n = 2, 4$ -particles. It is expected that the efficiency distribution is thus the same for these two pairs of parameters. When $n = 5$, we may notice that for EGE or csEGE, the distributions are the same for $k = 1, 5$ and $k = 2, 4$. For $k = 1, 5$, one difference between two matrices either in EGE or csEGE, one with $k = 1$ and the other with $k = 5$, is that the diagonal elements for $k = 1$ are sums of independent independent variables, while for $k = 5$ the diagonal elements are just independent random variables. For $k = 2, 4$, the k -body spaces have the same dimension, therefore the number of independent random variables is the same. This raises similarities in the matrix elements between $k = 2, 4$, although in general there is no particle-hole symmetry in these ensembles [72].

The next natural question is to ask which states are involved in the efficiencies obtained in Fig. 3.1. We will focus in the case $n = 5$, because this is the case in which we found the largest efficiencies compared to other values of n . Figure 3.2 shows the frequency histograms of the pair of states that give the best efficiency. The total number of states for either case, EGE or csEGE, is 10^4 (the number of realizations in each ensemble). In the $x - y$ plane we have the combination of states $|\mu\rangle$ and $|\nu\rangle$ for which we obtained $P_{\mu,\nu}$. Each column represents $k = 1, 3$ or $k = 5$. The top row corresponds to the EGE and the bottom row to the csEGE case. In the top row we can see that any combination of states $|\mu\rangle, |\nu\rangle$ can give a contribution to $P_{\mu,\nu}$. We further see that this does not depend on k , for all cases we obtain a similar frequency distribution. For the csEGE case (bottom row), we observe that only certain pair of states (again independent of k) contribute to the best efficiency, namely they can be either $|1\rangle$ and $|6\rangle$, $|2\rangle$ and $|5\rangle$, or $|3\rangle$ and $|4\rangle$. In other words, the only states that contribute to the best efficiency are those that are related by centrosymmetry in the n -particle space.

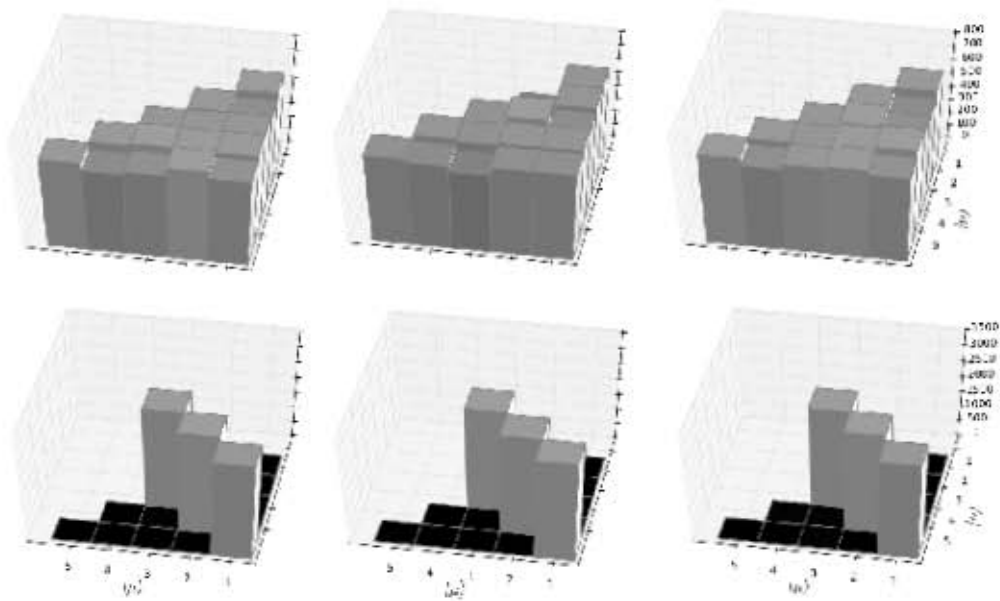


Figure 3.2: Frequency of states that participate in the best efficiency of Fig. 3.1. From left to right, $k = 1, 3, 5$. Top row: EGE model without centrosymmetry. Bottom row: EGE model with centrosymmetry. Notice that in the EGE case, any combination of states may participate in obtaining the efficiency \mathcal{P} . For the csEGE case, almost all efficiencies are obtained between the states that preserve centrosymmetry. The states related between each other are $|1\rangle$ and $|6\rangle$, $|2\rangle$ and $|5\rangle$, $|3\rangle$ and $|4\rangle$.

Chapter 4

Efficient open systems: Transport properties

As in the previous chapter, we analyse a fermionic spinless system with n -fermions distributed over l single-particle states. The basis in which we represent either a EGE or a csEGE is the occupation number basis (see Section 2.1.6). The crucial quantity for measuring efficiency in the open system using NEGF is the total current through the system (see Eq. (2.30))

$$I = \int_{-\infty}^{\infty} T(E) dE, \quad (4.1)$$

where $T(E) = \text{Tr}(\Gamma_S G \Gamma_D G^\dagger) = |2G(E)_{in,out}|^2$ is the transmission probability between the ingoing and outgoing states (Eq. (2.31)). Here, $G(E) = (E - H_k - \Sigma_S - \Sigma_D)^{-1}$ is the Green's function of the central system at the energy E (Eq. (2.15)). Recall that by Eq. (2.26), $\Gamma_{S/D} = i(\Sigma_{S/D} - \Sigma_{S/D}^\dagger) = 2 \text{Im}(\Sigma_{S/D})$. The position of the input contact is fixed to be $|1\rangle = |1, 1, \dots, 1, 0, 0, \dots, 0\rangle$, where all the fermions are shifted to the left. As the outgoing state we take $|N\rangle = |0, 0, \dots, 0, 1, 1, \dots, 1\rangle$, where all fermions are shifted to the right. These states are clearly related to each other by parity if H_k is centrosymmetric; see Fig. 4.1 for a schematic view of the scattering process

In the following analysis, the contacts are characterised by the self-energy matrix with elements

$$\Sigma_{(1 \text{ or } 6)r,s} = -i\eta\delta_{r,(1 \text{ or } 6)}\delta_{r,s}, \quad (4.2)$$

where η is the strength of the coupling which for now we set to $\eta = 1$.

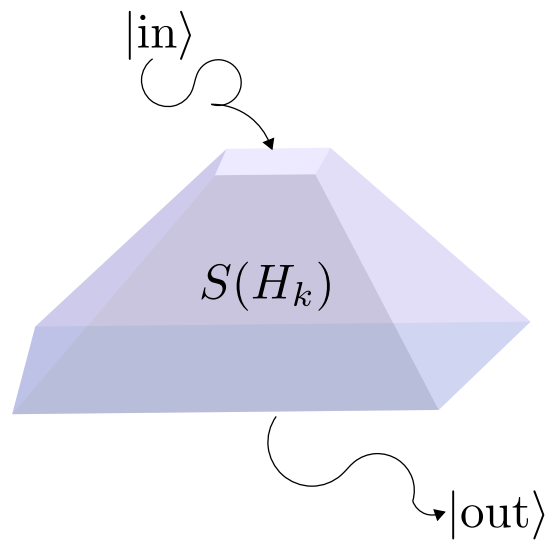


Figure 4.1: Schematic view of the scattering process. The input state $|\text{in}\rangle$ (i.e. the position where the source is attached to the system) suffers a scattering process S which depends on the random Hamiltonian H_k . The transmission probability (and total current) is measured at the output state $|\text{out}\rangle$, which is the position of the drain attached to the central system. The input state is the quantum many-body state $|1, 1, \dots, 1, 0, \dots, 0\rangle$ (i.e. the state where all fermions are shifted to the left), while the output state is $|0, 0, \dots, 0, 1, \dots, 1\rangle$ (all fermions are shifted to the right).

Before analysing the average quantities over the EGE or the csEGE, we present the typical behaviour for a single realization in each of these ensembles. For $l = 6$, $n = 5$ and $k = 3$, the energy resolved transmission $T(E)$ for two typical members of the ensemble is shown in Fig. 4.2.

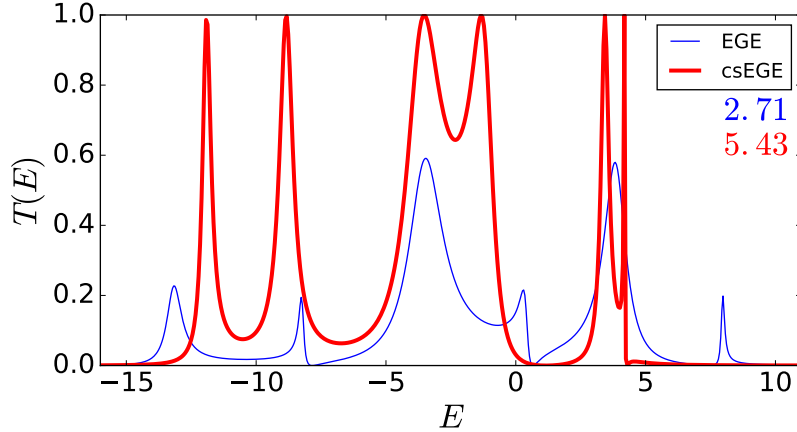


Figure 4.2: Transmission $T(E)$ as a function of the energy E for two typical members of each random matrix ensemble. The parameters are $l = 6$, $n = 5$, $k = 3$. In both cases resonances can be observed which are approximately at the eigenenergies of the central Hamiltonian. If the Hamiltonian is centrosymmetric (red/thick curve), we observe numerous resonances of perfect transport ($T = 1$). The transmission increases significantly compared to a Hamiltonian without this symmetry property (blue/thin curve). The blue and red numbers give the current for the EGE and the csEGE (Eq. (2.30)).

In both cases the transmission shows resonances which are located approximately at the eigenenergies of the Hamiltonian H_k . Many resonances of perfect transport ($T = 1$) can be observed if the Hamiltonian is centrosymmetric; see the red curve in Fig. 4.2. Our objective is not restricted to attain transmission $T(E) = 1$ at specific energy, but rather on improving the transport in the whole conduction band. We shall see that in general the transport properties are improved by imposing centrosymmetry. It is important to observe further features when comparing EGE versus csEGE. Note that in the csEGE case, the resonances are ~ 1 , while for the EGE case the resonances are < 1 . Note also that the peaks of such resonances are in general broader in the csEGE in comparison to those of the EGE case. Below we will see that even if we have broad peaks for the EGE, the contribution to the total current is not relevant because of the height associated to such peaks, which they are well below one. On the other hand, we will see that a csEGE have broad peaks, and also height ~ 1 . This means that broader peaks will contribute to more area below the transmission curve, which in turn implies more current (see Eq. (4.1)). This behaviour is also present when we analyse average currents over the ensemble for either of the two ensembles. Unless stated otherwise, for each concrete set of parameters, we have calculated an ensemble of 10^4 realizations with and without centrosymmetry being imposed.

4.1 Ensemble averaged transmission and current distributions

We have already seen in Fig. 4.2 that centrosymmetry enhances significantly the coherent transmission $T(E)$ through the system. The ensemble averaged transmission $\langle T(E) \rangle$ is displayed in Fig. 4.3, where all combinations of n and k are shown. We observe that in the case of centrosymmetric embedded Gaussian random matrix ensembles (csEGE) the average transmission is for all energies larger than for the non-centrosymmetric Gaussian ensembles (EGE), i.e. $\langle T_{\text{csEGE}}(E) \rangle > \langle T_{\text{EGE}}(E) \rangle$. In both cases the spectral span of the transmission, i.e., the width of the conduction band, is maximal for $k \sim n/2$ and increases with n . That is, the system is conductive for a wider range of energies. The ensemble averaged transmission is peaked around the center of the conduction band at $E = 0$.

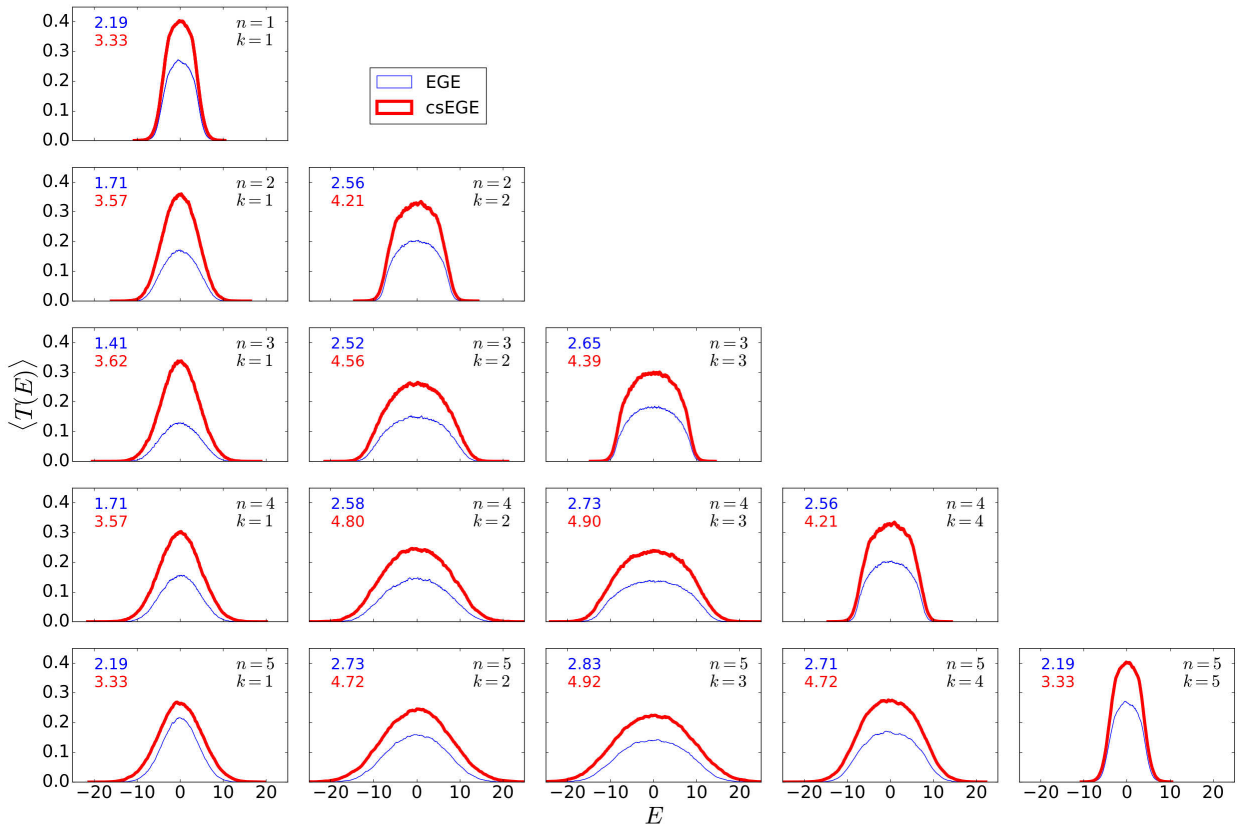


Figure 4.3: Ensemble averaged transmission $\langle T(E) \rangle$ as a function of the energy E for a system with $l = 6$ single-particle states. Each column has fixed value of k , for $k = 1, 2, \dots, n$, while each row corresponds to a fixed value of n , for $n = 1, 2, \dots, l - 1$. The ensemble consists of 10^4 realizations. The results corresponding to the EGEs are displayed by the blue/thin curves, while the red/thick curves illustrate the csEGEs results. The blue and red numbers give the mean averaged transmission for the EGE and csEGE respectively. Imposing centrosymmetry increases considerably the ensemble averaged transmission for all energies.

In particular, for fixed n (along a row in Fig. 4.3) maximal values of the transmission are attained at $k = 1$ and $k = n$ for the EGEs as well as for the csEGEs. The shape of the maxima differs in the two cases; for $k = 1$ the maximum is strongly peaked, whereas for $k = n$ it is broader and rounded. This behavior can be observed also for larger systems, see the Appendix, though the values for $k = 1$ are slightly larger than for $k = n$. All these cases ($l = 6, 8, 10$) are of interest because transport is typically more efficient in a narrow energy band around $E = 0$. This effect is most pronounced for the extrema at $k = n = 1$ and $k = n = 5$.

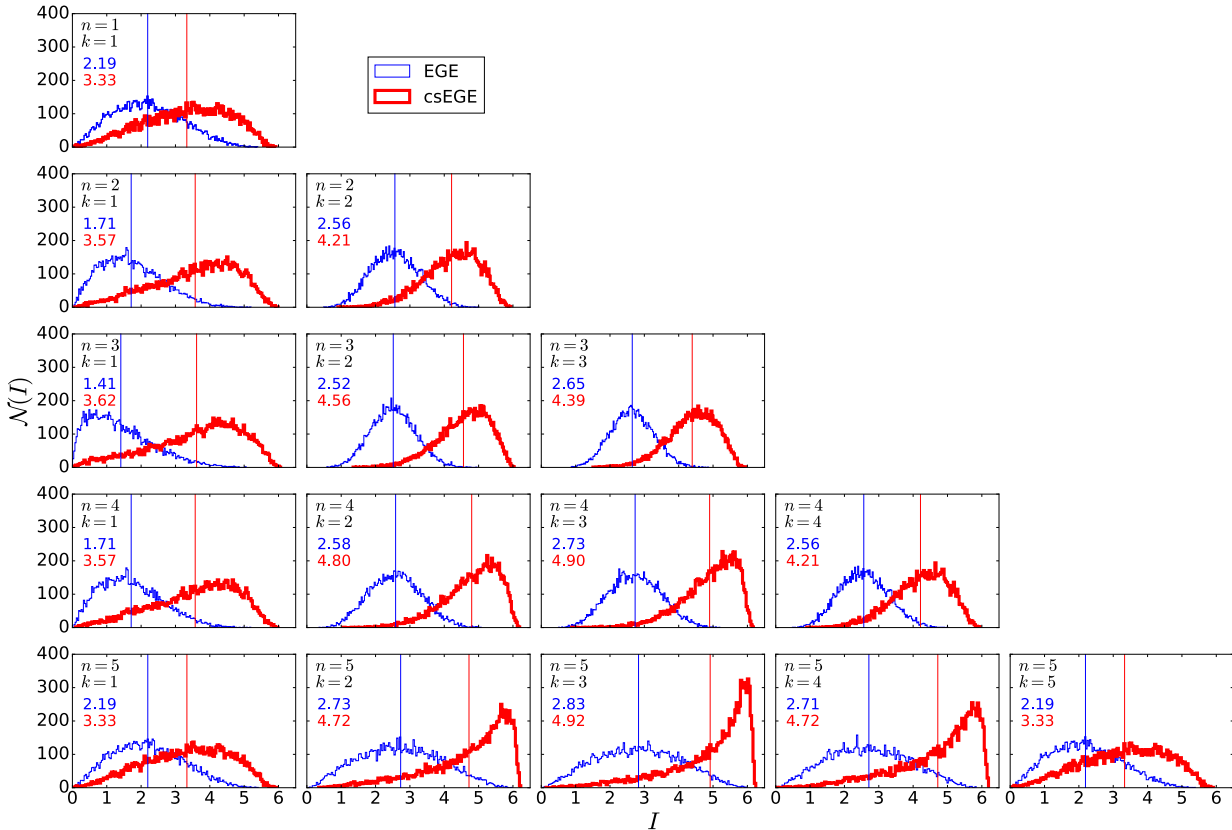


Figure 4.4: Frequency histogram of the current for 10^4 realizations for the EGE (blue) and the csEGE (red). The arrangement of the figures is the same as in Fig. 4.3. The average current $\langle I \rangle$ is indicated by blue and red vertical lines and their values are indicated in the insets. The current is maximal if the system is almost filled $n = l - 1$ and the rank of interaction between the particles is $k \sim n/2$.

In Fig. 4.4 we present the frequency histograms $\mathcal{N}(\mathcal{I})$ of the current, calculated by means of the Eq. (4.1). We observe that the average current $\langle I \rangle$, whose values are included in the insets and are illustrated by the vertical lines, is enhanced significantly when centrosymmetry is imposed. This trend is independent from the actual value of the parameters (n, k) . Moreover, the average current is maximal if the system is almost filled, i.e. $n = l - 1$, and the rank of interaction is $k \sim n/2$. These statements also apply to the mode (i.e. the position of the maximum) of the current distributions. Note that for larger systems (see the Appendix) the average

current is maximal for n close, but not identical, to $l-1$. These results for stationary transport are fully consistent with our previous results (see [50] and Fig. 3.1), where the dynamic propagation of states was addressed. The effects of centrosymmetry are thus present in time-dependent quantities [36, 37, 50] and also in stationary transport properties. We have shown that analysing the efficiency \mathcal{P} and the mean current $\langle I \rangle$ display similar features for the EGE compared to the csEGE. We can state that the transport is robust when we analyse time-dependent and time-independent quantities. Centrosymmetry enhances the transport either in the time (efficiency), or in transport in steady-state, and therefore could be used in every random system which meets the criteria of the csEGE. Returning to section 2.1.6 and to the related problems of engineering quantum systems [45, 51], the network flow problem in a disordered Hamiltonian system¹ can be enhanced by just imposing centrosymmetry.

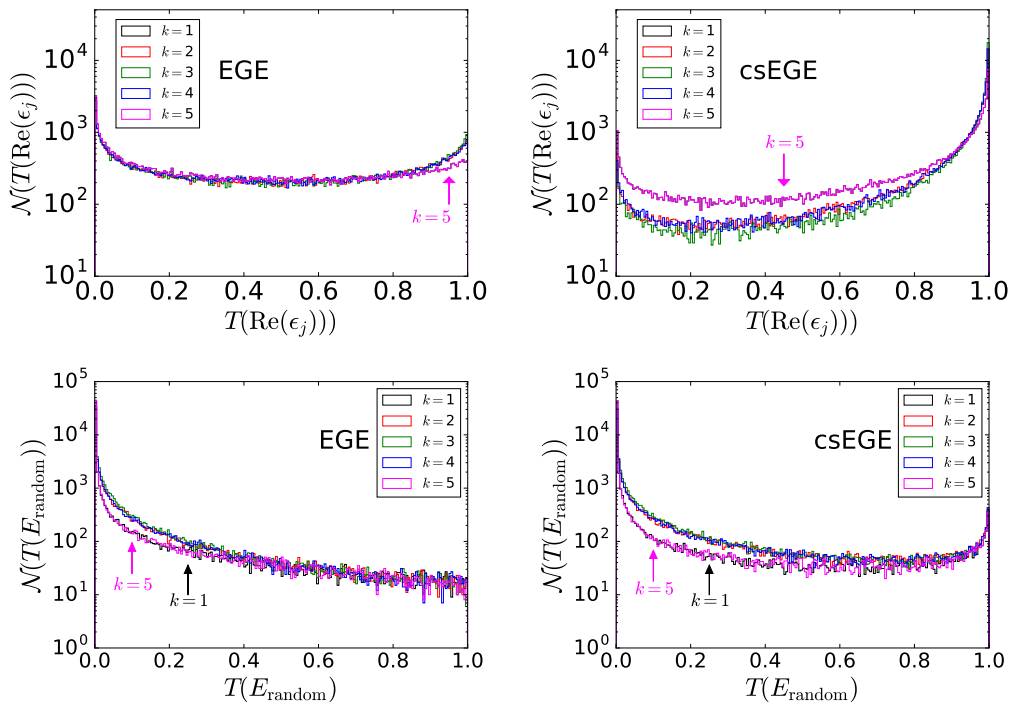


Figure 4.5: Top row: Histogram of the transmission evaluated at the real part of the complex eigenenergies of H'_k , where the resonances are approximately located. The histogram confirms our observation from Fig. 4.2 that centrosymmetry generates many resonances of optimal transmission $T(\text{Re}(\epsilon_j)) = 1$. Bottom row: The histogram of the transmission at random energies confirms this property and furthermore, shows the general trend that centrosymmetry enhances the transmission for all energies, see Fig. 4.3. Note that the vertical axes are in logarithmic scale.

Similar to what we observed in Fig. 3.1, for $k = n$, H_k is a member of the GOE, we observe the same symmetry in these cases, i.e. results for the parameters $(n, k = n)$ and $(l - n, k = l - n)$ are identical. This can be seen clearly in the ensemble averaged

¹By a Hamiltonian system we mean a weighted graph whose weighted connectivity matrix is real symmetric.

transmission as well as in the frequency histogram of the total current, see Figs. 4.3 and 4.4 as well as in the Appendix. Further symmetries can be observed only in the distribution of the total current (Fig. 4.4), where we observe numerically that the cases $(n, k = 1)$ and $(l - n, k = 1)$ are identical.

As illustrated in Fig. 4.2, we observe that centrosymmetry yields many resonance peaks with perfect transmission, i.e. $T = 1$; for EGE we may find some perfect transmission resonances, but it is not the typical case. Denoting by ϵ_j the eigenvalues of H'_k (where $H'_k = H_k + \Sigma_S + \Sigma_D$), these resonances are located at energies $E \approx \text{Re}(\epsilon_j)$. This motivates us to study in Fig. 4.5 the statistics of the transmission at these energies $\text{Re}(\epsilon_j)$ (top row), and compare them with the transmission at random energies (bottom row) for the EGE and the csEGE in the case $n = l - 1$ and all possible values of k . These histograms confirm our observation about Fig. 4.2 that centrosymmetry generates many resonances with perfect transmission. Note that perfect transmission is also observed when the transmission is evaluated at random values of the energy (within the conductance band); yet, the relative frequency is higher by about two orders of magnitude for the csEGE. We also note that there is a weak dependence on k , such that $k \sim n/2$ dominates for larger values of the transmission. These results show the general trend that centrosymmetry enhances the transmission for all energies, see Fig. 4.3, which implies a higher total current.

In Fig. 4.6 we show the distribution of $2G_{\text{in,out}}(\text{Re}(\epsilon_j))$ in the complex plane for $n = l - 1$ and all values of k . This quantity is of interest since its modulus squared gives the transmission through the system at $E = \text{Re}(\epsilon_j)$, i.e. $T(E) = |2G_{\text{in,out}}|^2$. As the transmission is bounded to values equal or less than 1, the data points are distributed inside the unit circle. Strong correlations between the real and imaginary part are observed for both EGE and csEGE. For the EGE (left column), the data points are clustered around the origin, which corresponds to transmission resonances with low conductance. In contrast, in the case of csEGE (right column), the data points display an accumulation on the boundary of the unit circle, around the poles, corresponding to resonances of optimal transmission. We can also see that this accumulation is larger for $k \sim n/2$.

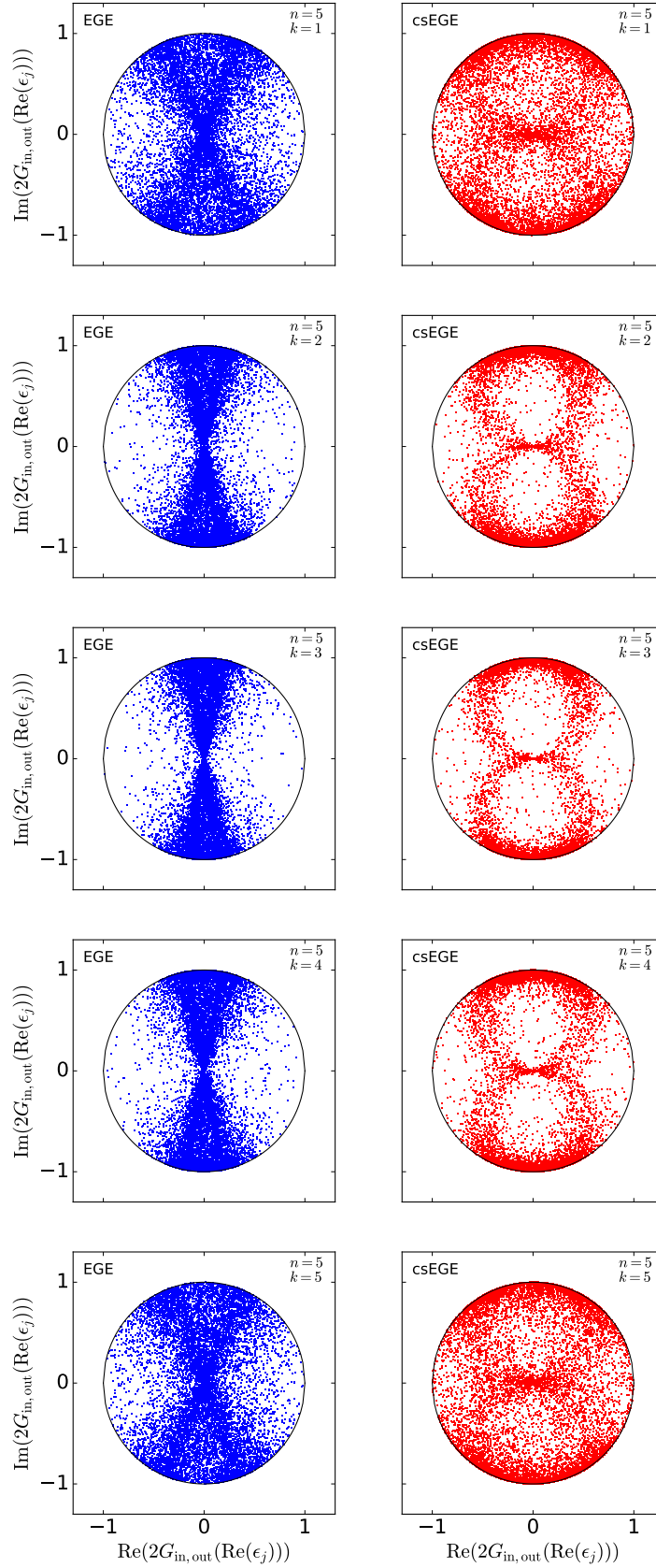


Figure 4.6: Distribution of $2G_{\text{in,out}}(\text{Re}(\epsilon_j))$ in the complex plane for 2000 realizations. Strong correlations between the real and imaginary part are observed in both cases. In the case of EGE (left column), data points are concentrated around the origin, which corresponds to transmission resonances of low conductance. For the csEGE (right column), the data points are accumulated on the poles, which corresponds to perfect transmission.

4.2 Statistics of the spectral decomposition of the transmission

In order to have more insight of the effects induced by centrosymmetry on transport, we use the spectral decomposition of the Green's function. Then, the transmission is expressed as

$$T(E) = |2G_{\text{in,out}}(E)|^2 = \left| \sum_{j=1}^N \frac{\Upsilon_j}{E - \epsilon_j} \right|^2, \quad (4.3)$$

where

$$\Upsilon_j \equiv 2\phi_{j,\text{in}}\phi_{j,\text{out}}. \quad (4.4)$$

Here, the $\phi_{j,\text{in}}$ or $\phi_{j,\text{out}}$ are the in/out components of the j th eigenfunction of the effective Hamiltonian H'_k . Note that H'_k is non-Hermitian but it has the property $H'_k{}^\dagger = H'_k{}^*$. In this case the eigenstates can be chosen in such a way that they fulfill the orthogonality relation $\langle \phi_i | \phi_j \rangle = \delta_{ij}$ and the completeness relation $1 = \sum_j |\phi_j\rangle \langle \phi_j|$, which have been used in Eq. (4.3).

In the following, we will focus on the case $n = l - 1 = 5$, which corresponds to the optimal case in terms of transport; see Figs. 4.3 and 4.4. Our results hold also for other n .

The real part of the complex eigenvalues ϵ_j determine the position of the transmission resonances; their distributions in terms of k , are shown in Fig. 2.4, last row. We observe that centrosymmetry has only weak effects; it increases marginally the spectral span. The differences between the two cases are decreasing when k increases. In both cases the spectral span is maximal for $k \sim n/2$. These observations explain that the width of the conduction band is maximal for $k \sim n/2$ and that it is marginally wider for the centrosymmetric case.

In turn, $\text{Im}(\epsilon_j)$ is related to the width of the transmission peaks, see Fig. 4.2. The distributions of $\text{Im}(\epsilon_j)$ are presented in Fig. 4.7. As shown, their structure is essentially independent of k . Comparing the EGE and csEGE cases we find that centrosymmetry amplifies the occurrence of the extrema: the number of eigenvalues with $\text{Im}(\epsilon_j) = 0$ and $\text{Im}(\epsilon_j) = -\eta = -1$ is larger when centrosymmetry is present. The former value corresponds to resonances of vanishing width, while the latter is related to broad resonances. Then, the histograms for the EGE show that the number of broad resonances vanishes linearly as $\text{Im}(\epsilon_j) \rightarrow -\eta$, while for the csEGE this limit attains a constant value.

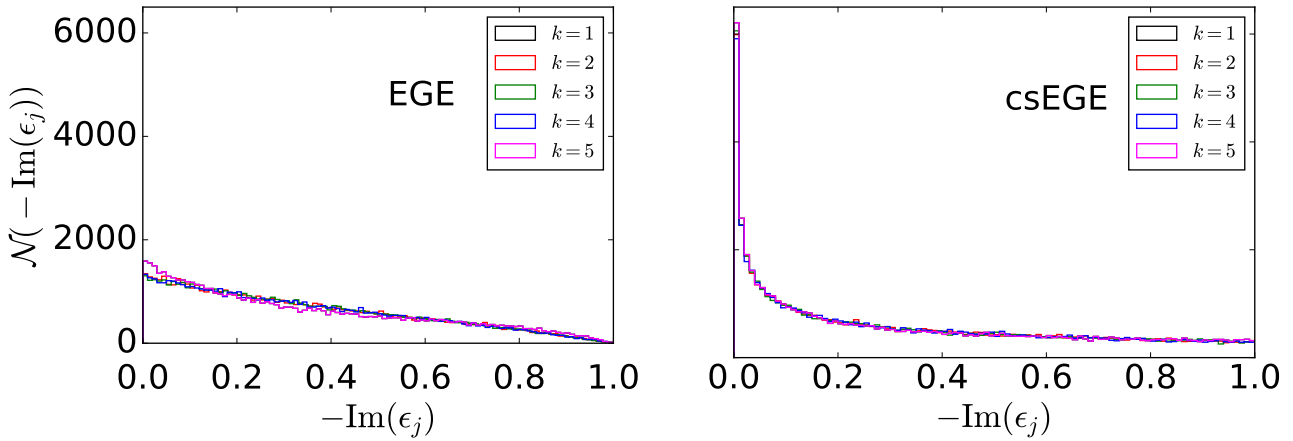


Figure 4.7: Distributions of $\text{Im}(\epsilon_j)$ for $n = l - 1 = 5$. The histograms are independent of the rank of interaction k , displaying a dependence on the presence or absence of centrosymmetry. Centrosymmetry enhances the number of eigenvalues with an imaginary part close to its minimum zero and its maximum $-\eta = -1$.

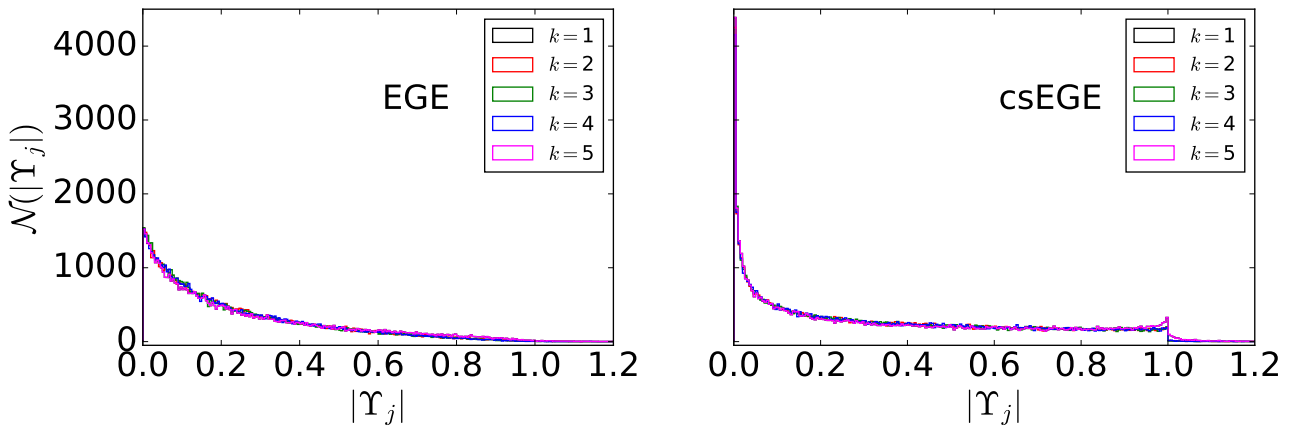


Figure 4.8: The histograms of $|\Upsilon_j|$ have similar properties as the histograms of $-\text{Im}(\epsilon_j)$ in Fig. 4.7.

The corresponding distributions Υ_j , see Eq. (4.4), is shown in Fig. 4.8. It displays similar properties as the distributions of $\text{Im}(\epsilon_j)$. That is, csEGE shows a larger frequency of events displaying zero and the maximal values of $|\Upsilon_j|$ than the EGE, and the distributions are essentially independent from k . This motivates us to investigate the correlations between $|\Upsilon_j|$ and $\text{Im}(\epsilon_j)$.

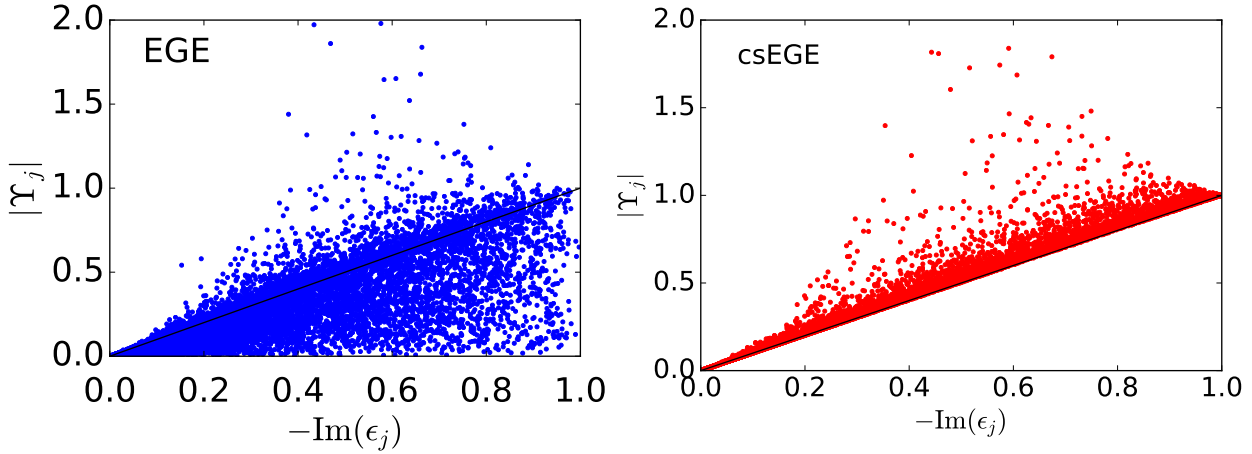


Figure 4.9: Distribution of $|\Upsilon_j|$ versus $-\text{Im}(\epsilon_j)$ for ensemble of 2000 realizations. Centrosymmetry imposes strong correlations. While in the case of arbitrary EGE the data points are located mainly in a triangle $|\Upsilon_j| \lesssim -\text{Im}(\epsilon_j)$, in the case of csEGE the data points are pinned on the line $|\Upsilon_j| \sim -\text{Im}(\epsilon_j)$ or above it.

In Fig. 4.9, we plot $|\Upsilon_j|$ versus $\text{Im}(\epsilon_j)$ illustrating strong correlations among these quantities. While in the EGE case the data points are scattered in the triangular region $|\Upsilon_j| \lesssim -\text{Im}(\epsilon_j)$, in the case of the csEGE the data appear on the line $|\Upsilon_j| \sim -\text{Im}(\epsilon_j)$ or above it.

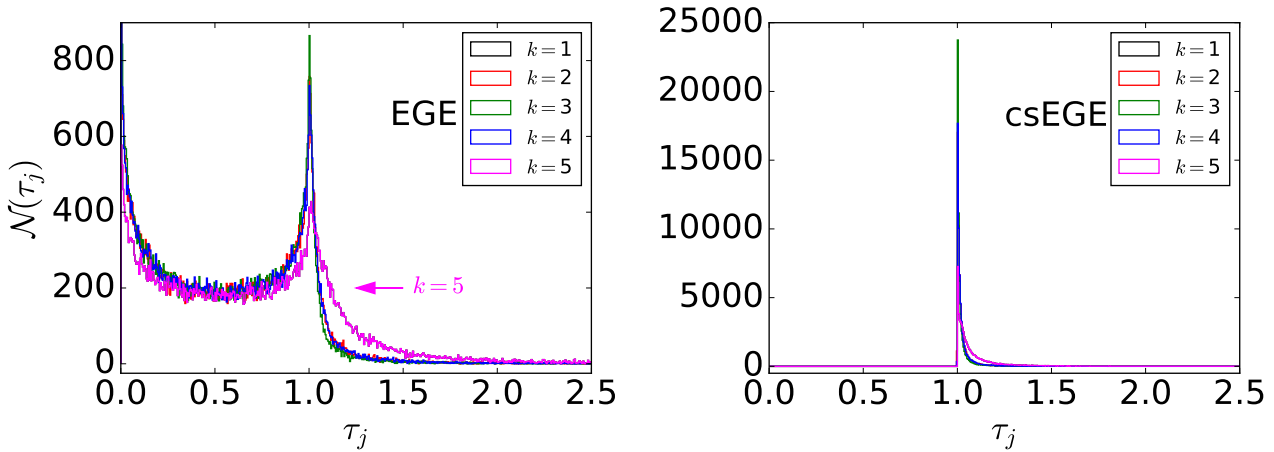


Figure 4.10: Histograms of the quotient $\tau_j \equiv |\Upsilon_j/\text{Im}(\epsilon_j)|$. For EGE this quotient is distributed mainly between 0 and 1 with maxima at these points. In contrast, for csEGE the distribution of τ_j is pinned to 1 without any value less than 1. This indicates the increase of resonances of perfect transmission due to centrosymmetry, see Fig. 4.5.

The histograms of the ratio $\tau_j \equiv |\Upsilon_j/\text{Im}(\epsilon_j)|$ in Fig. 4.10 show these strong correlations from another perspective. In view of Eq. (4.3), the quantity τ_j yields an

estimate of the transmission by taking into account the main resonance only and neglecting all interference effects, i.e. the other terms of the sum. For the EGE the distribution is mainly located between 0 and 1, with peaks at these values, dominated especially by the $k \sim n/2$ case. In turn, for the csEGE the values of τ_j are peaked strongly at 1 with a decaying tail beyond 1 but without any τ_j smaller than 1. Note also the difference in the vertical scales. The τ_j may attain values larger than 1 because the phases are neglected, which cause the transmission to be equal or less than 1. These two histograms close our statistical analysis to understand how centrosymmetry enhances transport. They confirm that centrosymmetry induces strong correlations which generate numerous transmission resonances of perfect transport ($T = 1$), see Fig. 4.5.

4.3 Current as a function of the coupling to the contacts

So far we have only considered that the coupling to the contacts is $\eta = 1$ (see Eq. (4.2)). Here, we address the effect in the transport properties if we change it. We focus on the case that the ensembles attains the best mean current $\langle I \rangle$, and therefore we set $l = 6$ and $n = 5$.

Figure 4.11 shows the mean current $\langle I \rangle$ as a function of the coupling parameter η . The left column indicates the case of the EGE and the right column for the csEGE. The scale in η of the top row is linear while in the bottom row the scale is logarithmic. The color code for the different values of k are in the figure caption. On all of the plots we can see that when $\eta = 1$, the mean current attains approximately the same value independent of the value of k . For all the four plots we can see that $k = 1, 5$ and $k = 2, 4$ display similar behaviour, and only for larger values of η they are slightly different. The case when $k = 3$ is the best to attain the largest current, either EGE or csEGE. On the other hand, the csEGE is always better than the EGE, regardless of the value of η . For the EGE case, we can improve $\langle I \rangle$ by $\sim 50\%$, and for the csEGE the current is improved by around 200%. We have thus found an interesting property not exploited before in the literature or experiments. A possibility to improve the transport properties in a disordered network is by tuning the coupling to the contacts (here represented by η).

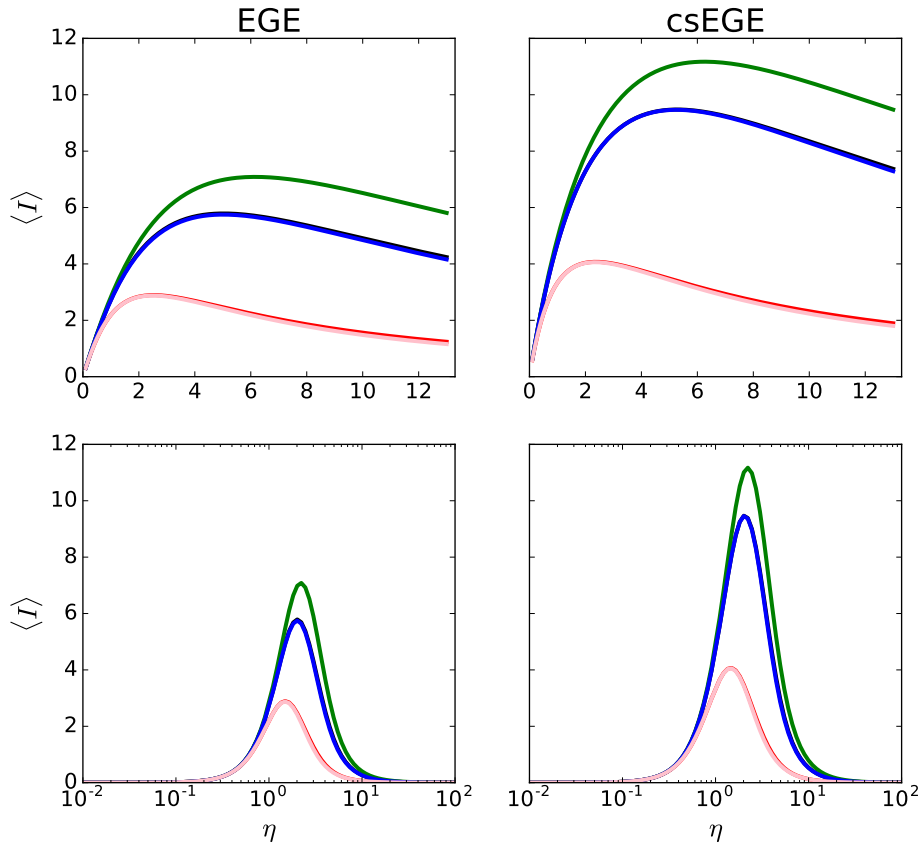


Figure 4.11: Mean current $\langle I \rangle$ as a function of the coupling parameter η . On the left column the EGE ensemble and on the right column the csEGE ensemble. The parameters are $l = 6$ and $n = 5$. Each color represents a different csEGE matrix: red, $k = 1$; black, $k = 2$; green, $k = 3$; blue, $k = 4$; pink, $k = 5$. There are 10^4 realizations in each ensemble. Notice that the upper row is a linear scale in η while the bottom row is a logarithmic scale.

Chapter 5

Centrosymmetry breaking and robustness

In this chapter we want to explore the effects of centrosymmetry breaking. Because of the different ways in which we can alter the centrosymmetric structure, we have divided this chapter into two sections. The first section describes how centrosymmetry can improve the transport from the EGE. In the second section, we will investigate how centrosymmetry can be broken and up to which point exists robustness (optimal transport properties) of this extra symmetry.

5.1 EGE to csEGE transition

As we saw in Chapters 3 and 4, the transport properties are essentially the same if we study the efficiency or the current through the ensemble. Therefore we will focus in the study of current for the EGE or the csEGE. In the first part we will introduce a Hamiltonian that takes into account the transition from EGE to csEGE as a function of a parameter ϵ and latter we analyse the transport properties as a function of ϵ .

The first thing to take into account is that the current depends on the distribution of energies over the ensemble, as it is given in Eq. (2.31). Our model to study EGE to csEGE current (or any other transition between embedded ensembles with or without centrosymmetry) must take into account the spectral span of those ensembles. A standard way to write such transition is

$$H = f(\epsilon)H_k + g(\epsilon)\tilde{H}_{k'}, \quad (5.1)$$

where H_k and $\tilde{H}_{k'}$ are matrices of the embedded ensembles with and without cen-

trosymmetry. The rank of interactions k and k' is taken from the interval $1, 2, \dots, n$. We have fixed the same l and n for both ensembles in order to have the same Hilbert space dimension in the n -particle space. f and g are functions of ϵ , which is a free parameter, and its job is to take us from system the H_k to system the $\tilde{H}_{k'}$. There are many ways to write these pair of functions, see for example [40], which is typical for studying systems with mean-field plus two-body interactions. In a similar spirit, we define such functions to be

$$\begin{aligned} f(\epsilon) &= \sqrt{1 - \epsilon}, \\ g(\epsilon) &= \sqrt{\epsilon}. \end{aligned} \tag{5.2}$$

Therefore our model to study transitions between EGE and csEGE reads

$$H = \sqrt{1 - \epsilon}H_k + \sqrt{\epsilon}\tilde{H}_{k'}. \tag{5.3}$$

A few remarks for choosing this form in f and g come in place. The first one is that, when $\epsilon = 0$, we recover H_k (a similar situation happens for $\tilde{H}_{k'}$ when $\epsilon = 1$). The next remark is the presence of the square roots. Suppose for the moment that both are EGE's and $k = k'$, and they are independent members of the ensemble. As we are dealing with ensembles of random matrices, the energy scale of H can be chosen via its spectral span, which is defined by $\text{var}(H) = \overline{\text{Tr}(H^2)}/N$, with N the Hilbert space dimension and Tr denotes the trace operation. In other words, the average energy density $\rho(E)$ (for the GOE) is given by the equation $\overline{\rho(E)} = \frac{1}{2N\pi\sigma^2}\sqrt{4N\sigma^2 - E^2}$ for $|E| \leq 2\sqrt{N\sigma^2}$, where σ is the standard deviation chosen for the (Gaussian!) matrix elements in H [7]¹. For $\sigma = 1$, as is our case, the average level density is precisely a semicircle and it is exactly this what we obtain when we fix $k = n$. Using the spectral span, we find

$$\begin{aligned} \text{var}(H) &= (1 - \epsilon) \times \text{var}(H_k) + \epsilon \times \text{var}(\tilde{H}_k) + 2\frac{\sqrt{(1 - \epsilon)\epsilon}}{N} \times \overline{\text{Tr}(H_k \times \tilde{H}_k)} \\ &= (1 - \epsilon) \times \text{var}(H_k) + \epsilon \times \text{var}(\tilde{H}_k), \end{aligned} \tag{5.4}$$

where in the first equality we have used the fact that H_k and \tilde{H}_k are uncorrelated members of the EGE², and therefore $\overline{\text{Tr}(H_k \times \tilde{H}_k)} = 0$. As we are in the case where $k = k'$, $\text{var}(H_k) = \text{var}(\tilde{H}_k)$ and therefore $\text{var}(H) = \text{var}(H_k)$. In other words, with this choice of the functions f and g we do not change the spectral span and therefore we do not modify the conduction band with the addition of the perturbation.

¹ Remember that the GOE has twice the variance in its diagonal elements.

²Note that for the csEGE we obtain a similar calculation.

5.1.1 Analysis of the results

Following section 5.1, we analyse the EGE to csEGE transition. To do so, we model this transition with Eq. (5.3)

$$H = \sqrt{1 - \epsilon}H_k + \sqrt{\epsilon}\tilde{H}_{k'}. \tag{5.3}$$

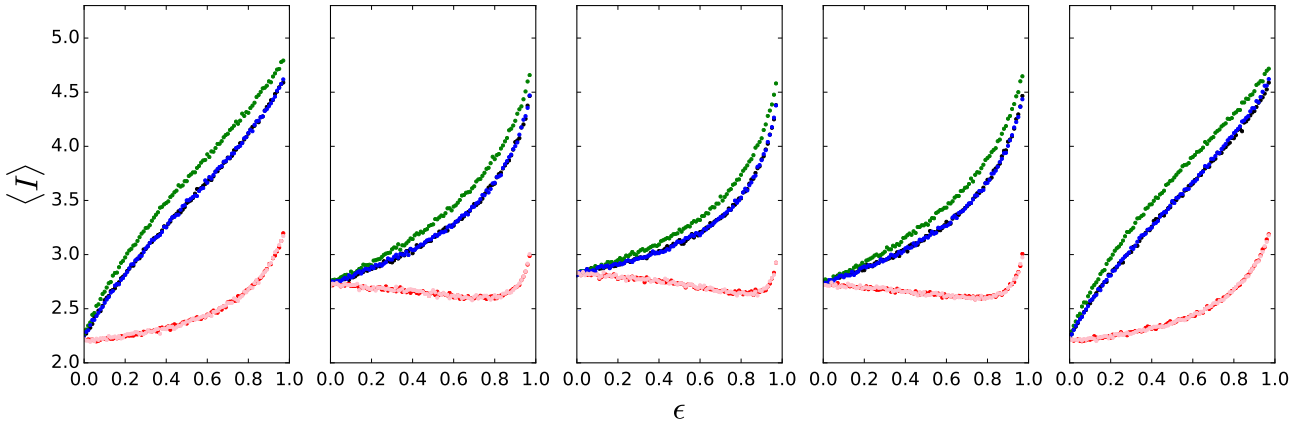


Figure 5.1: EGE to csEGE transition. The mean current $\langle I \rangle$ is plotted as a function of the transition parameter ϵ . From left to right, each plot represents a fixed k for the EGE. The colors label different ways to go from a fixed EGE k to a csEGE. Red is for the transition to csEGE with $k' = 1$; black for the csEGE with $k' = 2$; green for the csEGE with $k' = 3$; blue for the csEGE with $k' = 4$; and pink for the csEGE with $k' = 5$. The best case for the transition is $k' = 3$ (as expected). For $k' = 2, 3, 4$ the transition improves the total mean current. For EGE with $k' = 2, 3, 4$ and transition $k' = 1, 5$ there is a decay in $\langle I \rangle$, and for high values of ϵ this is surpassed.

Figure 5.1 explores this transition. The mean current $\langle I \rangle$ of the Hamiltonian H in Eq. (5.3) is plotted as a function of the parameter ϵ . We have fixed $l = 6$, $n = 5$ and we have considered 10^4 realizations. From left to right, each plot represents a fixed k in the EGE ensemble (first term of Eq. (5.3)). The possible values are again $k = 1, 2, 3, 4, 5$, one for each plot. The colors represent the different ways in which we can do the transition from a fixed k in the EGE to a csEGE. In red we have the transition to csEGE with $k' = 1$, in black to csEGE with $k' = 2$, in green to csEGE with $k' = 3$, in blue to csEGE with $k' = 4$, and in pink to csEGE with $k' = 5$. As it is to be expected, when $\epsilon = 0$ or 1 we recover the mean values for the current given in the Fig. 4.4, for the EGE or the csEGE respectively. For any value of k in the EGE, the best transition scenario corresponds to a perturbation of a csEGE with $k' = 3$. The cases $k' = 1, 5$ and $k' = 2, 4$ behave similarly (either with EGE or with csEGE), which is a feature already observed in Chapter 4. It is clear from the plots that a perturbation of a EGE with a csEGE and $k' = 2, 3, 4$ always yields better current. If we want to double the initial current we essentially

need that $\epsilon = 0.5$, when the EGE has $k = 1, 5$. While for EGE with $k = 1, 5$ the increase of the current is very rapid, for the EGE with $k = 2, 3, 4$ the increase is slower. What we are seeing in these cases is the effect of the centrosymmetry: for low values of ϵ the centrosymmetry does not dominate the transition, and it slowly starts to take over in the $\langle I \rangle$, until finally reaches its final value when $\epsilon = 1$. The situation is a little bit different when the perturbation is $k' = 1, 5$. When EGE has $k = 1, 5$, this perturbation slowly increases the current, but when EGE has values $k = 2, 3, 4$ the behaviour is completely different. In the latter case, it is clearly seen that the perturbation diminishes $\langle I \rangle$ as a function of ϵ . This trend is followed until $\epsilon \sim 0.9$, and then $\langle I \rangle$ slowly increments to its final value of ~ 3.3 . The reason is that the spectral span of the perturbation (and therefore the mean current) is smaller compared to the EGE with $k = 2, 3, 4$. Therefore we have a steady decrease in the mean current until we reach a minimum of ~ 2.6 . As it is to be expected, the case with $k = 3$ for EGE is the least affected.

To end this section, we point out that we can do the same analysis but reading the plots in Fig. 5.1 backwards. That is, these plots contain the information of centrosymmetry breaking when the perturbation is an arbitrary EGE. In the next section, we analyse the centrosymmetry breaking but by some specific perturbations. We shall look at parity breaking and block off-diagonal perturbations.

5.2 Centrosymmetry breaking

In section 2.1.3 we saw how to construct centrosymmetric ensembles from embedded ensembles. We found that, depending on the parameters (l, n, k) , the centrosymmetry can be full or partial. A quick look at Table 2.1.4 reveals the possible ways in which the combination of the parameters (l, n, k) may give rise to either partial, or full centrosymmetry, when $l = 6$. In this section we are interested in cases where there is full centrosymmetry in the n -particle space. Specially in the case $n = 5$, we can always find full centrosymmetry. The question addressed is how centrosymmetry breaking affects the transport properties of the central system H_k . In the following, we discuss different ways to break full centrosymmetry. From now on, we will use the term centrosymmetry to refer to full centrosymmetry (without referring to partial centrosymmetry). We will discuss only the case where the Hilbert space dimension N is of even dimension.

We recall the main definitions of centrosymmetry already addressed in Sec. 2.1.4. A centrosymmetric matrix is a matrix, say H , that commutes with the exchange matrix J . The exchange matrix is the matrix with entries $J_{i,j} = \delta_{i,N+1-j}$, where $\delta_{i,j}$ is the Kroenecker delta and N is the Hilbert space (even) of n particles distributed over l single-particle states. It can be shown that H has the block structure [75] (for odd dimension N , this block representation is a little bit different; we will deal

only with N even)

$$H = \begin{pmatrix} A & C^T \\ C & JAJ \end{pmatrix}, \quad (5.5)$$

where A and J are of dimension $N/2 \times N/2$ and $A = A^T$, $C^T = JCJ$, where we have denoted the matrix transpose operation with the superscript T . The matrix H can be written in block diagonal form via the transformation [75]

$$H' = KHK^T = \begin{pmatrix} A - JC & 0 \\ 0 & A + JC \end{pmatrix}, \quad (5.6)$$

where

$$K = \frac{1}{\sqrt{2}} \begin{pmatrix} \mathbb{1} & -J \\ \mathbb{1} & J \end{pmatrix}, \quad (5.7)$$

and $\mathbb{1}$, J are the identity matrix and the exchange matrix respectively, both of dimension $(N/2 \times N/2)$. Equation (5.6) shows that H' is composed of two correlated blocks. The eigenvectors of H' fulfill one of the following identities

$$\begin{aligned} Jv &= v, \\ Jw &= -w, \end{aligned} \quad (5.8)$$

which are called symmetric and skew-symmetric, correspondingly. There are $N/2$ symmetric and $N/2$ skew-symmetric eigenvectors. The last set of equations tell us that the eigenfunctions obey parity, in the sense of the exchange matrix J . Equation (5.6) can be therefore be interpreted as H' having parity and correlations in sectors of different symmetry, i.e. in sectors of even and odd subspaces (generated by its eigenvectors). The next natural question is how to break the parity and the block structure of H , i.e. the centrosymmetry breaking. The motivation for doing this is to quantify how much the transport properties of csEGE are robust against breaking the parity and correlations which are induced by centrosymmetry. We will explore two possible options, and we will describe them in what follows.

The first way to break the structure of the centrosymmetry is to break the block form of Eq. (5.6). Effectively this would be parity breaking. In the block diagonal basis, our system with perturbation takes the form

$$H'_{\text{perturbed}} = \alpha \begin{pmatrix} A - JC & 0 \\ 0 & A + JC \end{pmatrix} + \beta \begin{pmatrix} 0 & B \\ B & 0 \end{pmatrix}, \quad (5.9)$$

where B is a matrix of dimension $(N/2) \times (N/2)$ and will be a member of the GOE. The real parameters α and β will be determine in the following. In the original basis, this last equation takes the form

$$H_{perturbed} = \alpha \begin{pmatrix} A & C^T \\ C & JAJ \end{pmatrix} + \beta \begin{pmatrix} B & 0 \\ 0 & -JB.J \end{pmatrix} = \alpha H_k + \beta H(B), \quad (5.10)$$

where α and β are normalization constants which we choose to be $\alpha = \sqrt{1 - \epsilon}$ and $\beta = \sqrt{\epsilon}$.

Based on the previous B -perturbation, the second natural way to break the symmetry is to alter the block structure of Eq. (5.6) (forget for the moment the normalization constants). Instead of Eq. (5.9), our perturbation this time is

$$\tilde{H}_{perturbed} = \begin{pmatrix} A - JC & 0 \\ 0 & A + JC \end{pmatrix} + \begin{pmatrix} D_1 & 0 \\ 0 & D_2 \end{pmatrix}, \quad (5.11)$$

where the D_i matrices can be chosen each one independently from a GOE. Upon making the inverse transformation to the occupation number basis we find

$$\tilde{H}_{perturbed} = \begin{pmatrix} A + D_1 + D_2 & C^T + (D_2 - D_1)J \\ C + J(D_2 - D_1) & J(A + D_1 + D_2)J \end{pmatrix}. \quad (5.12)$$

Taking a closer look of this equation, we find that in this expression, the perturbation formula does not alter the centrosymmetric structure. The reason is that, in the block-diagonal basis, the perturbation

$$\begin{pmatrix} D_1 & 0 \\ 0 & D_2 \end{pmatrix}, \quad (5.13)$$

is centrosymmetric. This is the starting point of the analysis of [36].

The final way that we choose to break the centrosymmetry is to add, directly in the occupation number basis, the perturbation

$$\tilde{H}_{perturbed} = \alpha \begin{pmatrix} A & C^T \\ C & JAJ \end{pmatrix} + \beta \begin{pmatrix} 0 & D \\ D^T & 0 \end{pmatrix} = \alpha H_k + \beta H(D), \quad (5.14)$$

where now D is a real matrix with Gaussian normal variables in each entry. Again we choose similarly the normalization constants to be $\alpha = \sqrt{1 - \epsilon}$ and $\beta = \sqrt{\epsilon}$.

5.3 Centrosymmetry breaking in efficient csEGE networks

In the following we investigate centrosymmetry breaking in ensembles with full centrosymmetry. The best option for obtaining the optimal current is when $n = l - 1$, we have set in the following $l = 6$ and $n = 5$; which we call now efficient EGE networks.

5.3.1 Parity breaking

As we have discussed in section 5.2, centrosymmetry is essentially parity and correlations between sectors separated by parity. One option to break the centrosymmetry is breaking the parity, and we end up with Eq. (5.10)

$$H_{\text{perturbed}} = \sqrt{1 - \epsilon}H_k + \sqrt{\epsilon}H(B) \quad (5.10)$$

Here, ϵ is the perturbation strength and can take the values from zero (only the centrosymmetric matrix) to 1 (only the presence of the perturbation). By choosing ϵ in this way, we can investigate the whole transition from centrosymmetry to parity breaking.

Figure 5.2 shows the parity breaking scenario displaying the mean current $\langle I \rangle$ as a function of ϵ . The color code is in the figure caption. For any value of k , the perturbation diminishes significantly the mean current (up to $\epsilon \sim 0.2$). Then the decay is much slower and finally, from $\epsilon = 0.8$ the decay in the mean current is again significantly until it becomes zero. The reason that at the end we have zero current lies in the block structure of $H(B)$ (at $\epsilon = 1$). In other words, if we consider the graph structure of $H(B)$, essentially we have two disconnected graphs in the occupation number basis. One of the contacts is in one isolated graph and the other contact is in the other isolated graph. There is no chance for energy flow and therefore the current is suppressed. For $k = 1, 5$ the effect of parity breaking is rather strong. One reason is that, in the absence of $H(B)$, these are the two cases with smaller $\langle I \rangle$. The situation is improved for other values of k , and in fact the behaviour is not too different. The case which is less affected by the perturbation is $k = 3$, which is in agreement with previous results of transmission efficiency and $\langle I \rangle$. Following this similar trend, $k = 2, 4$ behave similarly, as well as $k = 1, 5$.

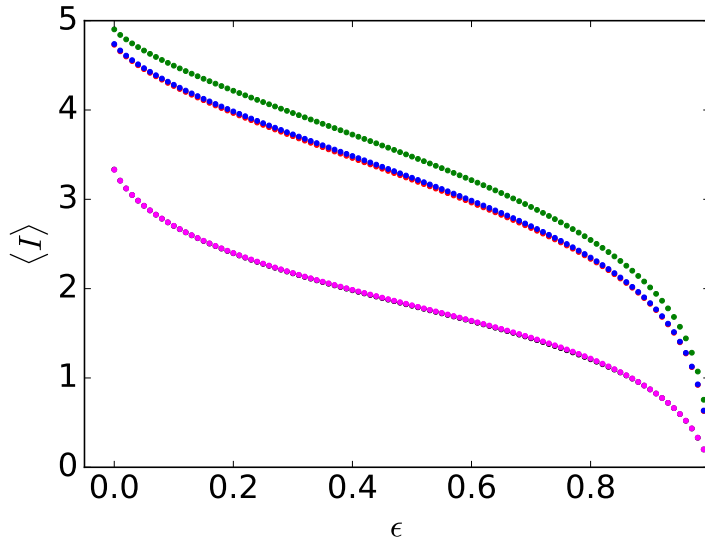


Figure 5.2: Parity breaking applied to centrosymmetry (see Eq. (5.10)) as a function of ϵ (perturbation strength) and $\langle I \rangle$ (mean current over the ensemble). The centrosymmetric part is chosen for the parameters $l = 6$ and $n = 5$. Each color represents a different csEGE matrix: black, $k = 1$; red, $k = 2$; green, $k = 3$; blue, $k = 4$; magenta, $k = 5$. There are 10^4 realizations in each ensemble. Notice that at first the perturbation affects significantly the centrosymmetric structure (up to 0.2), then the decay becomes more or less linear up to 0.8, and finally the decay is again significant up to current suppression, when $\epsilon = 1$.

5.3.2 Block perturbation in occupation number space

The second way to break the centrosymmetry is written in Eq. (5.14)

$$\tilde{H}_{perturbed} = \sqrt{1 - \epsilon}H_k + \sqrt{\epsilon}H(D) \quad (5.14)$$

Figure 5.3 shows the effect of symmetry breaking by applying the off-diagonal block perturbation with the matrices D . The color code is the same as in the previous figure. In this situation, for all k , the mean current $\langle I \rangle$ suffers a steady decrease, until it reaches its final value, which is when the perturbation $\tilde{H}_{perturbed}$ dominates. The quantity $\langle I \rangle$ is less affected when $k = 3$. When $k = 2, 4$ both curves follow a similar behaviour and $\langle I \rangle$ attain intermediate values. For $k = 1, 5$ the mean current decays less abruptly than in the previous cases. We can see that for all values of k , the perturbation affects the mean current. For $k = 2, 3, 4$, the mean current diminishes $\sim 50\%$, and for $k = 1, 5$ it only diminishes $\sim 33\%$. This gives us the insight that for $k = 1, 5$, the system is more robust in the presence of $H(D)$.

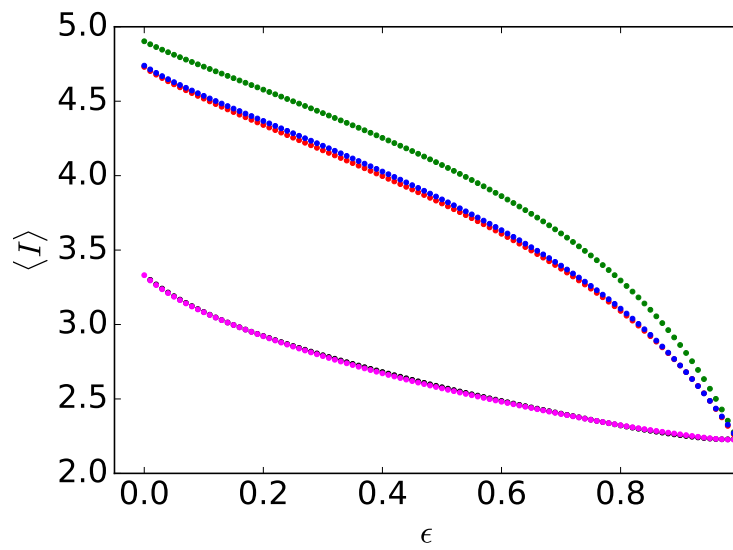


Figure 5.3: Centrosymmetry breaking (see Eq. (5.14)) as a function of ϵ (perturbation strength) and $\langle I \rangle$ (mean current over the ensemble). The centrosymmetric part is chosen for the parameters $l = 6$ and $n = 5$. Each color represents a different csEGE matrix: black, $k = 1$; red, $k = 2$; green, $k = 3$; blue, $k = 4$; magenta, $k = 5$. There are 10^4 realizations of each ensemble. In this case (any k), the mean current $\langle I \rangle$ is diminished in every case until it reaches a minimum.

Chapter 6

Conclusions and outlook

In this thesis we have analysed transport properties in small disordered networks. The networks were generated considering a physical system composed by fermions, distributed over l -single particle states. The interactions are random and are given by the Embedded Gaussian Ensemble (EGE). The randomness in the interactions are responsible for the disorder. The aim was to compare transport properties of both closed and open systems, and also in short time scales of time and in the steady-state. We have found that transport benefits when we impose the centrosymmetry on the Embedded Ensembles. This gives further evidence to determine that disordered networks as we constructed them, display transport properties that are robust to different time scales, and also are robust despite the interaction with external systems. Before describing the specific conclusions for the different parts of the thesis, we recall that random matrix models (as those studied here) describe generic quantum systems classified by their global symmetries. Inspired by the nuclei, the usual requirement for applying RMT to realistic situations is to have a complex many-body interacting quantum system. While it would be possible to solve such problems for the low energies part of the spectrum, usually it is almost impossible to describe them for high excitation energies. One then replaces the complicated interaction Hamiltonian by an ensemble of systems that *in average* describe the behaviour of the system. The whole work in this thesis is in describing this ensemble approach, and certainly opens the possibility to use the knowledge acquired for a more realistic application. In our specific case, random matrices generically describe disordered systems that may be found in nature, like the FMO complex or quantum buses under noise influence. Certainly, random matrices and localization theory are closely related (e.g. see [6, 93]) and in a way they culminate with the work done by Efetov [94]. Our approach here is different from localization theory, in the sense that, having a model for studying disorder we pose the following question: what are the minimum requirements in which, despite of disorder, we can still obtain good transport properties? We believe that our results answer greatly this enquiry. The improvement relies in the imposition of an extra symmetry (centrosymmetry!), which is needed to overcome localisation.

In the following we describe the specific conclusions for each of the chapters in the thesis. First we studied the distribution of quantum efficiencies in disordered networks with many-body interactions, whose structure is modeled by the embedded Gaussian ensemble. In particular, we studied the role played by centrosymmetry, which is defined at the one-particle space, and then extended to the k - and n -particle spaces. We have shown that (full) centrosymmetry enhances the efficiencies dramatically, being a requirement to have non-zero probability for Perfect State Transfer (PST) [45, 46]; the lack of centrosymmetry yields comparatively poor efficiencies. We note that centrosymmetry is introduced at the one-particle level, and then extended to the k - and n -body space. The rank of the interaction which displays the highest probability that the best efficiency \mathcal{P} is above the benchmark value corresponds to $k \sim n/2$ (for $n = l - 1$). The pairs of states that yield the best efficiencies appear uniformly among those states linked by centrosymmetry. Previous results have shown that random perturbations on networks with PST destroy or affect significantly this property; for details see [52, 95] and also [51] and references therein. Our results show that, despite of the random character of the k -body interactions that we have considered, certain n -body networks display good efficiencies and may attain near perfect state transfer with non-zero probability. Our results could be exploited as new design principles of networks with good efficiency, which is preserved under certain many-body random perturbations. For instance, considering the implementation of efficient quantum wires, it may be interesting to consider the case of filling factors that are smaller but close to one, where many-body interactions yield very good efficiencies. Finally, the results open the possibility to understand the good efficiency properties experimentally observed in exciton transport in biological systems, such as the Fenna-Matthews-Olson (FMO) complex [3, 96, 97]. One possible starting point would be to study the efficiency transport of the FMO complex. Its Hamiltonian is in the literature (see for example [31]). A quick inspection of the Hamiltonian reveals that the errors $\pm\Delta$ in its matrix elements are relevant (and also the diagonal elements contain more degree of error than the off-diagonal ones) and could be taken into account into a stochastic model. To do so, one would have to use this Hamiltonian and the errors could be modeled using constant probability distribution between $\pm\Delta$. We can construct then a stochastic ensemble based on real data. The next step would be to measure transport efficiency and current distributions. This leads us to the second part of our conclusions when we analysed the open system by using the NEGF method.

In the second part of the thesis we have analysed the stationary transport properties of fermions through small disordered interacting networks, again modeled by embedded Gaussian ensembles of random matrices. We have addressed the influence of centrosymmetry and have shown that the transport is enhanced significantly if centrosymmetry is present. This applies for the transmission $T(E)$, which is a function of the energy of the excitation, as well as for the averaged total current I through the system (see Figs. 4.3 and 4.4, respectively). We have shown that centrosymmetry induces many transmission resonances of perfect transport ($T = 1$), which enhances the transport in the overall conduction band (see Figs. 4.2 and 4.5). We have also seen that, independently of whether the system is centrosymmetric or not,

the width of the conduction band is maximal for $k \sim n/2$ and increases with n until the system is almost filled. In contrast, for $k = 1$ and $k = n$ the conduction band width is minimal. In the best case, which appears when the system is almost filled $n = l - 1$ and the rank of interaction is $k \sim n/2$, centrosymmetry enhances the averaged total current by 75% and its mode increases by a factor of 2. For larger systems (see the Appendix), the best cases appear for values of n close to but less than $l - 1$; the improvement of the transport by centrosymmetry is even stronger. Moreover, we observe that the distribution of the total current for the csEGE has a very large dominating peak for $n = l - 1$, close to the highest observed currents. Our results are therefore in perfect agreement with the analysis of transmission efficiency. Using the spectral decomposition of the Greens function, we have shown that centrosymmetry enhances the extrema (see Figs. 4.7 and 4.8). The number of resonances with minimal (0) and maximal (1) width (proportional to $\text{Im}(\epsilon_j)$) and weight (proportional to $|\Upsilon_j|$) increases. Centrosymmetry also induces strong correlations between the width and the weight of the resonances (see Figs. 4.9 and 4.5). This suppresses destructive interference effects in the system and thus causes backscattering-free transmission resonances, which enhance the overall transport. We interpret these results as a manifestation that centrosymmetry is an important property for the design of quantum networks with efficient transport characteristics. So far we have not taken into account the presence of decoherence, which will be inevitably present in biomolecules at room temperature, and to some extent, also in quantum devices. Therefore an open question is to consider how to introduce the dephasing effect in our model.

We next analysed the centrosymmetry robustness against perturbations in Chapter 5. To begin with, we analysed in section 5.1.1 the EGE to csEGE transition. When we use as a perturbation a csEGE with $k' = 2, 3, 4$, we can always improve the mean current $\langle I \rangle$. The degree of this improvement also depends if the system with $\epsilon = 0$ (perturbation parameter) is an EGE with $k = 1, 5$ or with $k = 2, 3, 4$. The primary reason is the spectral span which implies a bigger conduction band for $k' = 2, 3, 4$, while for $k' = 1, 5$ the conduction band is smaller. The only drawback in perturbing with a csEGE is when $k' = 1, 5$. In these cases, the spectral span plays a detrimental role in the mean current. We found a steady decrease until we reach a minimum, and only for high values of ϵ we can find a small increase in the mean current. If we read the results starting from $\epsilon = 1$, we can also study centrosymmetry breaking by a general EGE with a fixed k . In this case, the perturbation decreases very fast the mean current. The correlations in the csEGE are very sensitive to a general perturbation chosen from the EGE. In the subsequent section we investigated two ways to break the centrosymmetry. Centrosymmetry could be seen as parity and correlation between elements of distinct parity sectors. We proceeded in the first part of section 5.3 to investigate the parity breaking. We could observe three regimes as a function of the strength parameter for the perturbation. The first regime is a fast decay in the mean current $\langle I \rangle$. Afterwards there is an approximate linear decay regime for almost all values of the strength transition. Finally the mean current decays faster to zero. In this case the current is suppressed because there are no edges connecting the two (isolated) graphs of our network. Despite the fact that

with $k = 3$ we obtained the biggest mean current without perturbation, in this case the best escenario is when the interaction is set to $k = 3$. We then analysed the centrosymmetry breaking by a block anti-diagonal perturbation. In this case, $k = 3$ remains as the best case to obtain the largest mean current, for all values of the perturbation. We highlight that this is to be expected, since the total Hamiltonian was chosen to have the same spectral span as $H_{k=3}$. As in the previous case, there is a decrease of the mean current, more intense for $k = 2, 3, 4$, and less for $k = 1, 5$.

We finish this section by adding a final comment on centrosymmetry. Our analysis has compared when centrosymmetry is present versus when it is absent. We have found that centrosymmetry is a desirable property to have in a disordered system. Centrosymmetry is also present in Perfect State Transfer [45, 46] and efficient transport in the GOE [36]. In all these three cases, it seems that it is necessary to demand centrosymmetry as a design principle. However, it is known that molecular complexes also fulfill this property, and therefore centrosymmetry is an inherent property of certain biosystems (see for example [98]). Therefore, our results are not only candidates for application in engineered quantum systems, but also are applicable to systems that actually exist in nature.

Appendices

Appendix A

Bigger systems

A.1 Systems with $l = 8$ and $l = 10$ single-particle states

In this appendix we show, equivalently to Figs. 4.3 and 4.4, the ensemble-averaged transmission and the frequency histogram of the total current for systems consisting of $l = 8$ (Figs. A.1, A.3, respectively) and $l = 10$ (Figs. 14 and 15, respectively) single-particle states. Note that, although we have added only up to four single-particle states to the system studied in the main text, the dimension of the Hilbert space $\binom{l}{n}$ is up to 10 times larger. Note also that the spectral span, the width of the conduction band, and hence the total current increase with l (see [72]). We observe qualitatively the same properties as for the smaller system with $l = 6$, except that maximal values of the total current are observed also for fillings close to but less than $l - 1$. The mode of the distribution of the total current for the csEGE is strongly peaked for $n = l - 1$, close to the highest observed currents. The statistics of the spectral decomposition is the same as for the system discussed in the main text.

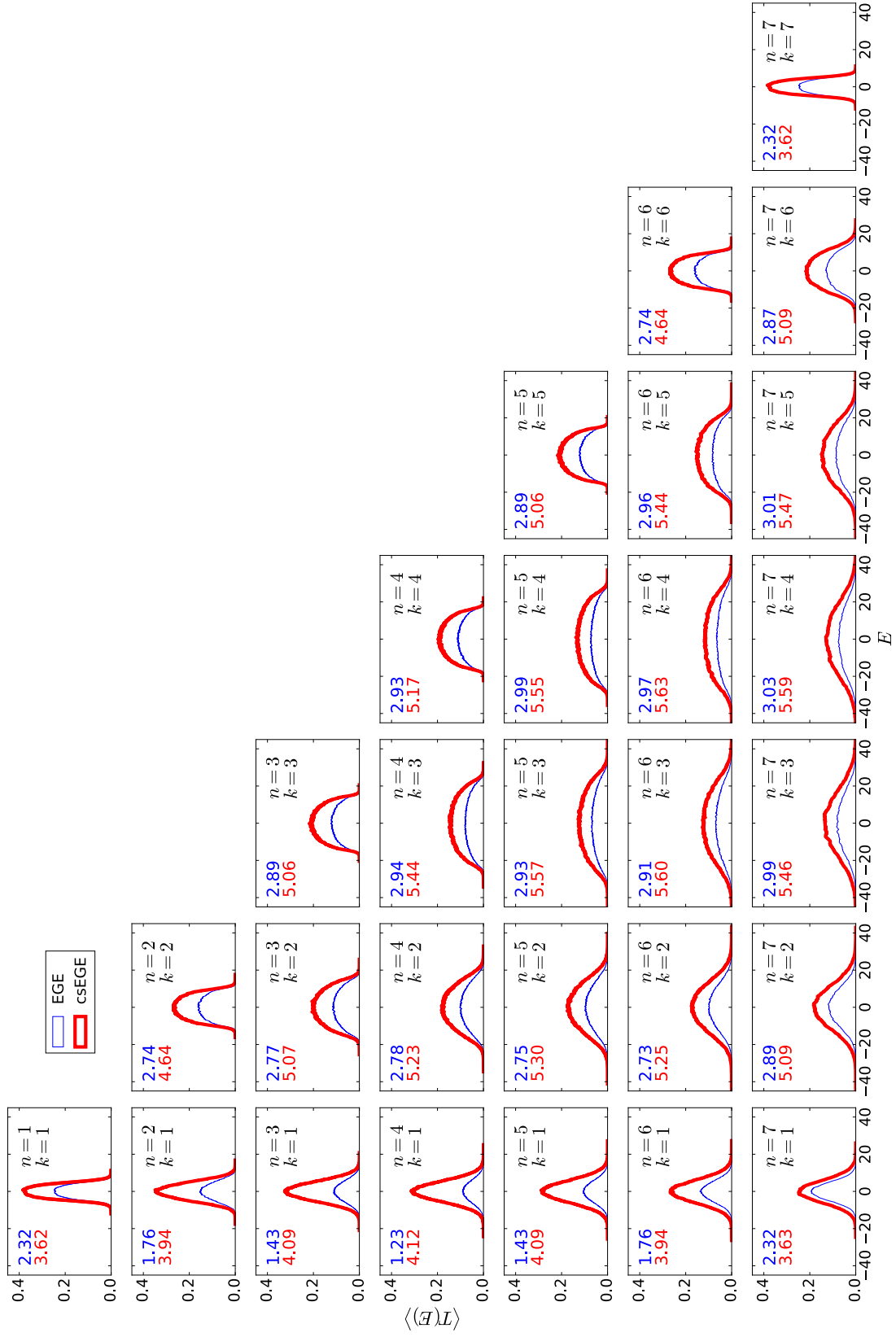


Figure A.1: Ensemble-averaged transmission $\langle T(E) \rangle$ for a system with $l = 8$ single-particle states. The arrangement of the figures is the same as in Fig. 4.3



Figure A.2: Frequency histogram of the current for a system with $l = 8$. The arrangement of the figures is the same as in Fig. 4.4.

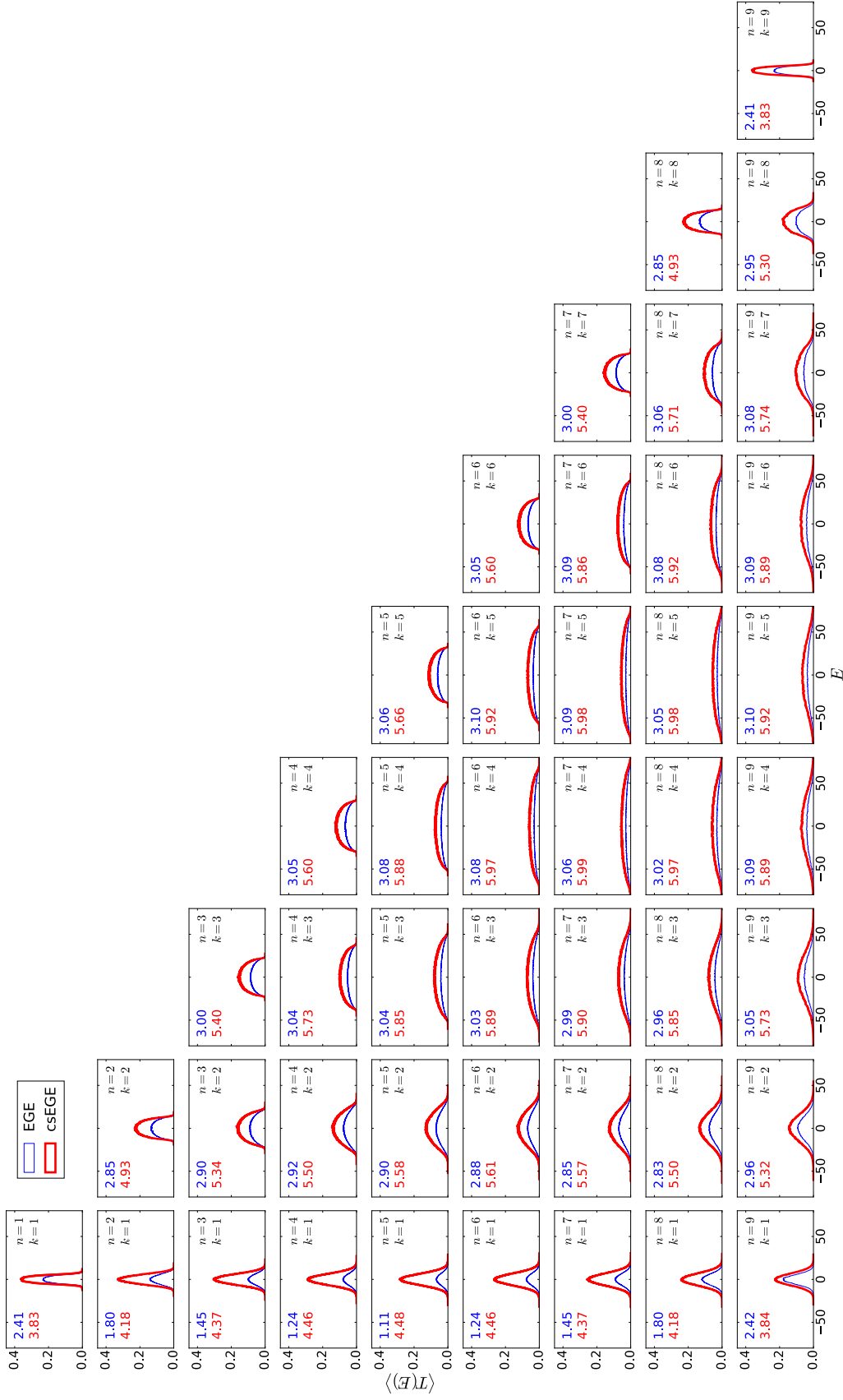


Figure A.3: Ensemble-averaged transmission $T(E)$ for a system with $l = 10$. The arrangement of the figures is the same as in Fig. 4.3.

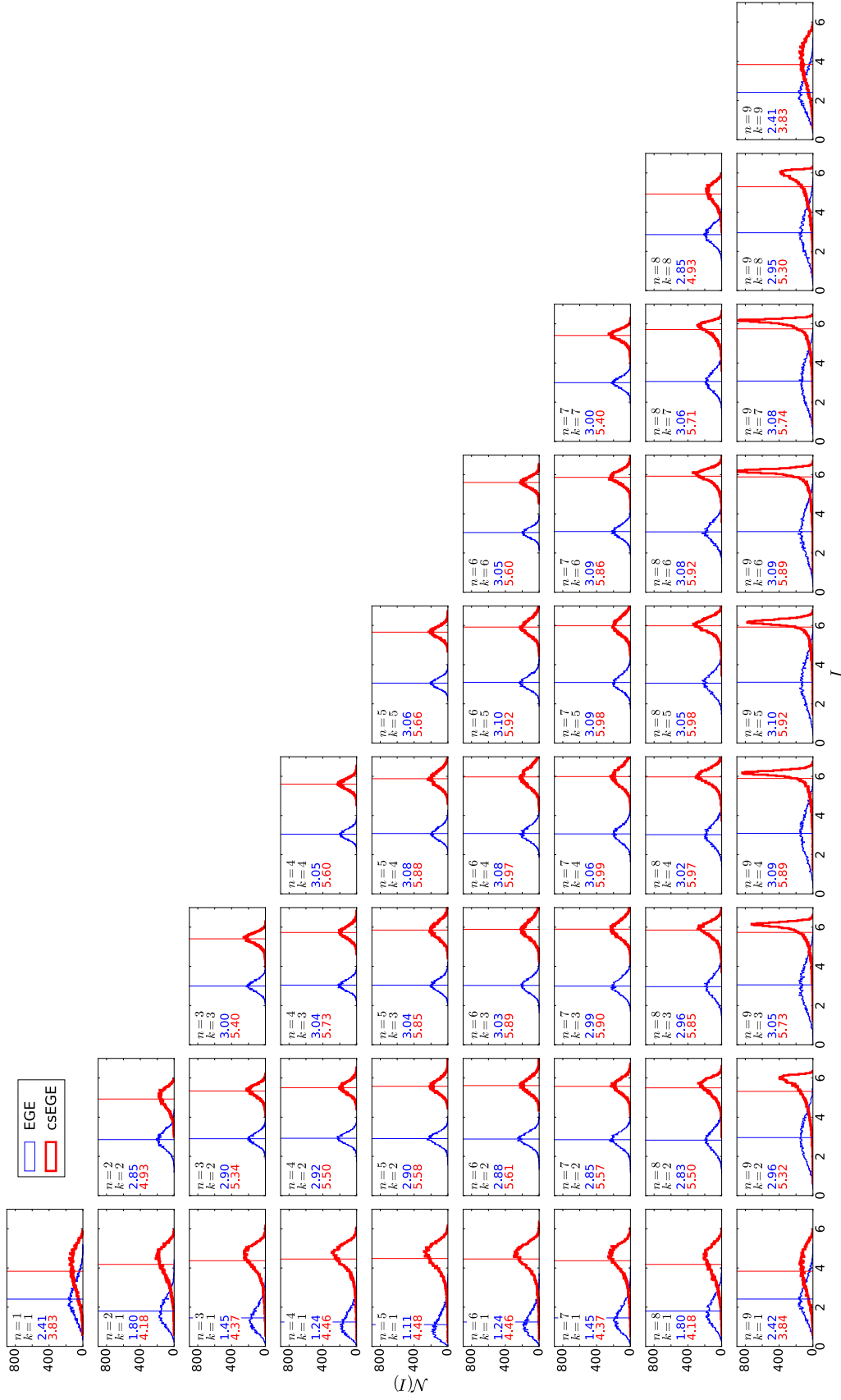


Figure A.4: Frequency histogram of the current for a system with $l = 10$. The arrangement of the figures is the same as in Fig. 4.4.

Appendix B

Publications

The thesis is based mainly in the following list of publications done by the author and contributors.

- Adrian Ortega, Manan Vyas and Luis Benet. *Quantum efficiencies in finite disordered networks connected by many-body interactions*. Annalen der Physik, Vol. 527, Issue 9-10, October 2015, Pages 748-756.
- Adrian Ortega, Thomas Stegmann and Luis Benet. *Efficient quantum transport in disordered interacting many-body networks*. Physical Review E, Vol. 94, Issue 4, October 2016, Pages 042102.

Bibliography

- [1] P. W. Anderson, *Phys Rev* **109**, 1492 (1958).
- [2] M. Walschaers, F. Schlawin, T. Wellens, and A. Buchleitner, *Annual Rev. Cond. Matt.* **7**, 223 (2016).
- [3] R. E. Fenna and B. W. Matthews, *Nature* **258**, 573 (1975).
- [4] S. Bose, *Contemporary Physics* **48**, 13 (2007).
- [5] T. A. Brody, J. Flores, J. B. French, P. A. Mello, A. Pandey, and S. S. M. Wong, *Rev. Mod. Phys.* **53**, 385 (1981).
- [6] T. Guhr, A. Müller-Groeling, and H. A. Weidenmüller, *Phys. Rep.* **299**, 189 (1998).
- [7] O. Bohigas and M.-J. Giannoni, “Chaotic motion and random matrix theories,” (1984).
- [8] J. Adolphs and T. Renger, *Biophysical Journal* **91**, 2778 (2006).
- [9] P. Huo and D. F. Coker, *The Journal of Physical Chemistry Letters* **2**, 825 (2011).
- [10] S. I. Vulto, M. A. de Baat, R. J. Louwe, H. P. Permentler, T. Neefd, M. Miller, H. van Amerongen, and T. J. Aartsma, *The Journal of Physical Chemistry B* **102**, 9577 (1998).
- [11] J. Moix, J. Wu, P. Huo, D. Coker, and J. Cao, *The Journal of Physical Chemistry Letters* **2**, 3045 (2011).
- [12] G. S. E. Dugan Hayes, *Biophysical Journal* **100**, 20432052 (2011).
- [13] A. Ishizaki and G. R. Fleming, *Proceedings of the National Academy of Sciences* **106**, 17255 (2009).
- [14] M. Wendling, M. A. Przyjalowski, D. Gülen, S. I. E. Vulto, T. J. Aartsma, R. van Grondelle, and H. van Amerongen, *Photosynthesis Research* **71**, 99 (2002).
- [15] T. J. A. Craddock, D. Friesen, J. Mane, Stuart Hameroff, and J. A. Tuszynski, *Journal of the Royal Society Interface* **11**, (2014).

- [16] C. Kreisbeck, T. Kramer, and A. Aspuru-Guzik, *Journal of Chemical Theory and Computation* **10**, 4045 (2014), pMID: 26588548.
- [17] M. S. am Busch, F. Mh, M. E.-A. Madjet, and T. Renger, *The Journal of Physical Chemistry Letters* **2**, 93 (2011).
- [18] T. Zech, R. Mulet, T. Wellens, and A. Buchleitner, Pre-print -, (2012).
- [19] C. Curutchet, V. I. Novoderezhkin, J. Kongsted, A. Muoz-Losa, R. van Grondelle, G. D. Scholes, and B. Mennucci, *The Journal of Physical Chemistry B* **117**, 4263 (2013), pMID: 22992117.
- [20] A. Kell, R. E. Blankenship, and R. Jankowiak, *The Journal of Physical Chemistry A* **120**, 6146 (2016), pMID: 27438068.
- [21] V. Novoderezhkin, A. Marin, and R. van Grondelle, *Phys. Chem. Chem. Phys.* **13**, 17093 (2011).
- [22] H. van Amerongen and R. van Grondelle, *The Journal of Physical Chemistry B* **105**, 604 (2001).
- [23] V. Novoderezhkin, J. M. Salverda, H. van Amerongen, and R. van Grondelle, *The Journal of Physical Chemistry B* **107**, 1893 (2003).
- [24] G. S. Schlau-Cohen, T. R. Calhoun, N. S. Ginsberg, E. L. Read, M. Ballottari, R. Bassi, R. van Grondelle, and G. R. Fleming, *The Journal of Physical Chemistry B* **113**, 15352 (2009), pMID: 19856954.
- [25] F. J. Kleima, M. Wendling, E. Hofmann, E. J. G. Peterman, R. van Grondelle, and H. van Amerongen, *Biochemistry* **39**, 5184 (2000), pMID: 10819986.
- [26] J. R. Durrant, D. R. Klug, S. L. Kwa, R. van Grondelle, G. Porter, and J. P. Dekker, *Proceedings of the National Academy of Sciences* **92**, 4798 (1995).
- [27] K. Acharya, B. Neupane, V. Zazubovich, R. T. Sayre, R. Picorel, M. Seibert, and R. Jankowiak, *The Journal of Physical Chemistry B* **116**, 3890 (2012), pMID: 22397491.
- [28] V. I. Novoderezhkin, J. P. Dekker, and R. van Grondelle, *Biophysical Journal* **93**, 1293 (2007).
- [29] V. I. Novoderezhkin, E. Romero, J. P. Dekker, and R. van Grondelle, *ChemPhysChem* **12**, 681 (2011).
- [30] T. Zech, *Hidden Symmetries of Quantum Transport in Photosynthesis*, Master's thesis, Albert-Ludwigs-Universität Freiburg, Germany (2012).
- [31] T. Scholak, *Transport and coherence in disordered networks*, Ph.D. thesis, Albert-Ludwigs-Universität Freiburg, Germany (2011).
- [32] M. Milder, B. Brüggemann, R. van Grondelle, and J. Herek, *Photosynth Res* **104**, 257 (2010).

- [33] M. B. Plenio and S. F. Huelga, *New J. of Phys.* **10**, 113019 (2008).
- [34] P. Rebentrost, M. Mohseni, I. Kassal, S. Lloyd, and A. Aspuru-Guzik, *New J. of Phys.* **11**, 033003 (2009).
- [35] R. d. J. León-Montiel and J. P. Torres, *Phys. Rev. Lett.* **110**, 218101 (2013).
- [36] M. Walschaers, J. F.-d.-C. Diaz, R. Mulet, and A. Buchleitner, *Phys. Rev. Lett.* **111**, 180601 (2013).
- [37] M. Walschaers, R. Mulet, T. Wellens, and A. Buchleitner, *Phys. Rev. E* **91**, 042137 (2015).
- [38] T. Asaga, L. Benet, T. Rupp, and H. A. Weidenmüller, *Ann. Phys. (N.Y.)* **298**, 229 (2002).
- [39] L. Benet, S. Hernández-Quiroz, and T. H. Seligman, *Phys. Rev. E* **83**, 056216/1 (2011).
- [40] M. Vyas, V. Kota, and N. Chavda, *Physical Review E* **81**, 036212 (2010).
- [41] R. Blakenship, *Molecular mechanisms of photosynthesis* (Blackwell Science, 2002).
- [42] J. C. Cuevas and E. Scheer, *Molecular Electronics: An Introduction to Theory and Experiment* (World Scientific, 2010).
- [43] R. Portugal, *Quantum walks and search algorithms* (Springer, 2013).
- [44] S. Bose, *Phys. Rev. Lett.* **91**, 207901/1 (2003).
- [45] M. Christandl, N. Datta, A. Ekert, and A. J. Landahl, *Phys. Rev. Lett.* **92**, 187902 (2004).
- [46] M. Christandl, N. Datta, T. C. Dorlas, A. Ekert, A. Kay, and A. J. Landahl, *Phys. Rev. A* **71**, 032312 (2005).
- [47] R. Hammack, W. Imrich, and S. Klavžar, *Handbook of product graphs*, 2nd ed. (CRC Press, 2011).
- [48] A. Childs, R. Cleve, E. Deotto, E. Farhi, S. Gutmann, and D. Spielman, *Proc. 35th ACM Symp. Theory of Computing*, 59 (2003).
- [49] A. Bondy and U. Murty, *Graph Theory*, 3rd ed. (Springer, 2008).
- [50] A. Ortega, M. Vyas, and L. Benet, *Annalen der Physik* **527**, 748 (2015).
- [51] G. M. Nikolopoulos and I. Jex, *Quantum State Transfer and Network Engineering* (Springer, 2014).
- [52] A. Casaccino, S. Lloyd, S. Mancini, and S. Severini, *Int. J. Quantum Inf.* **7**, 1417 (2009).

- [53] G. Nikolopoulos, *Phys. Rev. A* **87**, 042311 (2013).
- [54] L. Benet and H. A. Weidenmüller, *J. Phys. A* **36**, 3569 (2003).
- [55] V. K. B. Kota, *Embedded Random Matrix Ensembles in Quantum Physics* (Springer, 2014).
- [56] E. P. Wigner, *Ann. of Math* , 36 (1951).
- [57] E. P. Wigner, *Proc. Cam. Phil. Soc.* **47** (1951).
- [58] M. L. Mehta, *Random Matrices*, 2nd ed. (Academic, New York, 1991).
- [59] A. M. Tulino and S. Verdú, *Random Matrix Theory and wireless communications* (now Publishers Inc., 2004).
- [60] Vinayak and T. Seligman, *AIP Conference Proceedings* **1575**, 196 (2014).
- [61] F. Mezzadri and N. Snaith, *Recent perspectives in Random Matrix Theory and Number Theory*, 1st ed. (Cambridge University Press, 2005).
- [62] H.-J. Stöckmann, *Quantum Chaos. An Introduction* (Cambridge University Press, 2000).
- [63] F. Peter J., *Log-gases and Random Matrices*, 1st ed. (Princeton University Press, 2010).
- [64] G. Akemann, J. Baik, and P. D. Francesco, *The Oxford Handbook of Random Matrix Theory*, reprint ed. (Oxford University Press, 2015).
- [65] B. French and S. S. M. Wong, *Phys. Lett. B* **449** (1970).
- [66] O. Bohigas and J. Flores, *Phys. Lett. B* **34**, 261 (1971).
- [67] J. Flores, M. Horoi, M. Müller, and T. H. Seligman, *Phys. Rev. E* **63**, 026204 (2001).
- [68] K. K. Mon and J. B. French, *Ann. Phys. (N.Y.)* **95**, 90 (1975).
- [69] T. Asaga, L. Benet, T. Rupp, and H. A. Weidenmüller, *EPL* **56**, 340 (2001).
- [70] R. Balian, *Il Nuovo Cimento B* **57**, 183 (1966).
- [71] G. R. Fleming, S. F. Huelga, and M. B. Plenio, *New Journal of Physics* **13**, 115002 (2011).
- [72] L. Benet, T. Rupp, and H. A. Weidenmüller, *Ann. Phys. (N.Y.)* **292**, 67 (2001).
- [73] T. Zech, R. Mulet, T. Wellens, and A. Buchleitner, *New J. Phys.* **16**, 055002 (2014).
- [74] A. Ortega, T. Stegmann, and L. Benet, *Phys. Rev. E* **94**, 12 (2016).
- [75] A. Cantoni and P. Butler, *Linear Algebra and its Applications* **13**, 275 (1976).

- [76] D. B. West, *Introduction to graph theory*, 2nd ed. (Prentice Hall, 2001).
- [77] H. Wilf, *Algorithms and Complexity*, internet edition ed. (A K Peters/CRC Press, 1994).
- [78] T. Scholak, F. de Melo, T. Wellens, F. Mintert, and A. Buchleitner, *Phys. Rev. E* **83**, 021912 (2011).
- [79] G. M. Nikolopoulos and I. Jex, eds., *Quantum State Transfer and Network Engineering*, 1st ed. (Springer, 2014).
- [80] R. Alicki and M. Fannes, *Quantum dynamical systems*, 1st ed. (Oxford University Press, 2001).
- [81] R. A. Horn and C. R. Johnson, *Matrix Analysis*, revised ed. (Cambridge University Press, 1990).
- [82] M. Di Ventra, *Electrical Transport in Nanoscale Systems* (Cambridge University Press, 2008).
- [83] T. Stegmann, O. Ujsághy, and D. E. Wolf, *Eur. Phys. J. B* **87**, 30 (2014).
- [84] T. Stegmann, M. Zilly, O. Ujsághy, and D. E. Wolf, *Eur. Phys. J. B* **85**, 264 (2012).
- [85] T. Stegmann, *Quantum transport in nanostructures: From the effects of decoherence on localization to magnetotransport in two-dimensional electron systems*, Ph.D. thesis, University Duisburg-Essen (2014).
- [86] S. Datta, *Electronic Transport in Mesoscopic Systems* (Cambridge University Press, 1997).
- [87] S. Datta, *Quantum Transport: Atom to Transistor*, 1st ed. (Cambridge University Press, 2005).
- [88] S. Datta, *Lessons from nanoelectronics*, 3rd ed. (World Scientific, 2012).
- [89] E. N. Economou, *Green's Functions in Quantum Physics*, 3rd ed. (Springer, 2006).
- [90] P. Mello and N. Kumar, *Quantum Transport in Mesoscopic Systems*, 1st ed. (Oxford University Press, 2004).
- [91] R. Landauer, *IBM J. Res. Dev.* **1**, 223 (1957).
- [92] T. Scholak, T. Wellens, and A. Buchleitner, *EPL* **96** (2011).
- [93] C. W. J. Beenakker, *Rev. Mod. Phys.* **69**, 731 (1997).
- [94] K. Efetov, *Supersymmetry in disorder and chaos*, 1st ed. (Cambridge University Press, 1999).

- [95] G. De Chiara, D. Rossini, S. Montangero, and R. Fazio, *Phys. Rev. A* **72**, 012323/1 (2005).
- [96] H. Lee, Y.-C. Cheng, and G. R. Fleming, *Science* **316**, 1462 (2007).
- [97] U. Würfel, M. Thorwart, and E. R. Weber, eds., *Semiconductors and Semimetals*, 1st ed. (Elsevier, 2011).
- [98] R. A. Molina, E. Benito-Matías, A. D. Somoza, L. Chen, and Y. Zhao, *Phys. Rev. E* **85**, 046118 (2012).